HHS Public Access

Author manuscript

Immunity. Author manuscript; available in PMC 2020 November 19.

Published in final edited form as:

Immunity. 2019 November 19; 51(5): 871–884.e6. doi:10.1016/j.immuni.2019.09.014.

Metabolite-sensing receptor Ffar2 regulates colonic group 3 innate lymphoid cells and gut immunity

Eunyoung Chun[1], **Sydney Lavoie**[1], **Diogo Fonseca-Pereira**[1], **Sena Bae**[1], **Monia Michaud**[1], **Hamid R. Hoveyda**[2], **Graeme L. Fraser**[3], **Carey Ann Gallini Comeau**[1], **Jonathan N. Glickman**[4,5], **Miles H. Fuller**[6], **Brian T. Layden**[7,8], **Wendy S. Garrett**[1,9,10,11,*]

[1]Departments of Immunology and Infectious Diseases and Genetics and Complex Diseases, Harvard T. H. Chan School of Public Health, Boston, MA, 02115, USA

[2]Euroscreen SA, 6041 Gosselies, Belgium

[3]EPICS SA, 6041 Gosselies, Belgium

[4]Department of Pathology, Harvard Medical School, Boston, MA, 02115, USA

[5]Beth Israel Deaconess Medical Center, Boston, MA, 02215, USA

[6]Department of Medicine, Northwestern University Feinberg School of Medicine, Chicago, IL, 60611, USA

[7]Division of Endocrinology, Diabetes, and Metabolism, University of Illinois at Chicago, Chicago, IL, 60612, USA

[8]Jesse Brown Veterans Affairs Medical Center, Chicago, IL, 60612, USA

[9]Broad Institute of Harvard and MIT, Cambridge, MA, 02142, USA

[10]Department of Medical Oncology, Dana-Farber Cancer Institute, Boston, MA, 02215, USA

[11]Lead Contact

SUMMARY

Group 3 innate lymphoid cells (ILC3s) sense environmental signals that are critical for gut homeostasis and host defense. However, the metabolite-sensing G-protein-coupled receptors that regulate colonic ILC3s remain poorly understood. We found that colonic ILC3s expressed *Ffar2*, a

*Correspondence: wgarrett@hsph.harvard.edu.

AUTHOR CONTRIBUTIONS

E.C., S.L, M.M. and D.F.-P. performed experiments and analyzed data; S.B. and E.C. performed RNA-Seq data analyses; H.R.H. and G.L.F. invented and provided the Ffar2 agonist used in this study; J.N.G. evaluated colitis scores; B.T.L. and M.H.F. provided *Ffar2*$^{fl/fl}$ mice; C.G.C. generated *Rorc-cre* x *Ffar2*$^{fl/fl}$ mice; E.C. and W.S.G. designed experiments, interpreted data and wrote the manuscript.

COMPETING FINANCIAL INTERESTS

The authors declare no competing financial interests. W.S.G. is on the SAB of Kintai Therapeutics, Leap Therapeutics, and Evelo Biosciences. G.L.F. is Chief Scientific Advisor at EPICS SA, the company with proprietary rights to the Ffar2 agonist (Patent No. WO 2011/076732 A1) used herein.

microbial metabolite-sensing receptor, and that Ffar2 agonism promoted ILC3 expansion and function. Deletion of *Ffar2* in ILC3s decreased their *in situ* proliferation and ILC3-derived interleukin-22 (IL-22) production. This led to impaired gut epithelial function characterized by altered mucus-associated proteins and antimicrobial peptides and increased susceptibility to colonic injury and bacterial infection. Ffar2 increased IL-22^{+} CCR6^{+} ILC3s and influenced ILC3 abundance in colonic lymphoid tissues. Ffar2 agonism differentially activated AKT or ERK signaling and increased ILC3-derived IL-22 via an AKT and STAT3 axis. Our findings suggest that Ffar2 regulates colonic ILC3 proliferation and function and identify an ILC3-receptor signaling pathway modulating gut homeostasis and pathogen defense.

Graphical Abstract

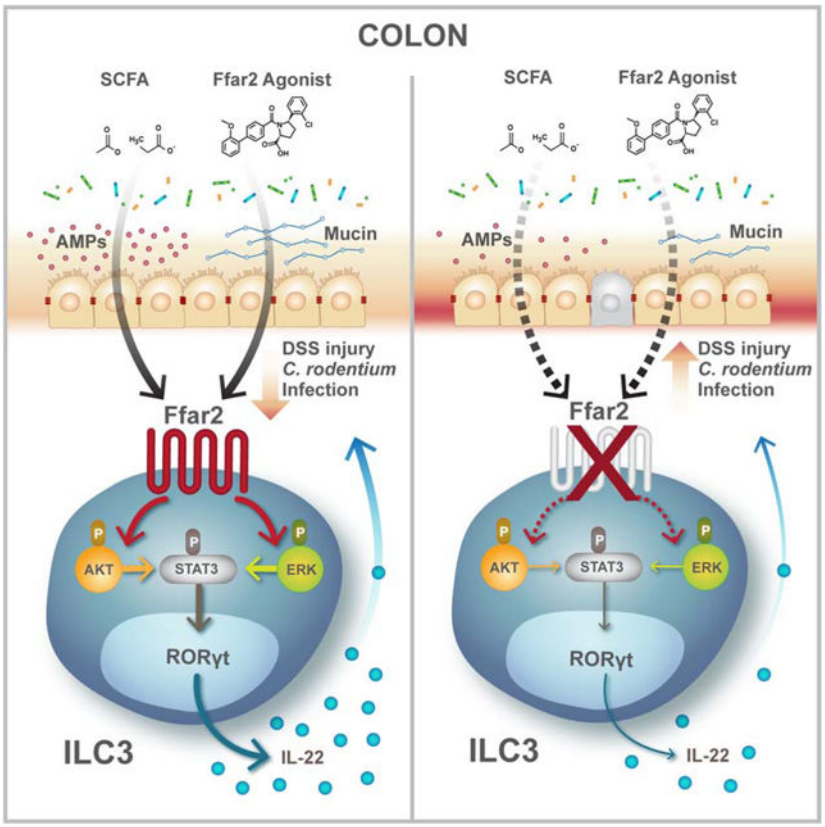

eTOC/In Brief

ILC3s are critical for gut homeostasis and host defense. Chun et al. unveil a role for the metabolite-sensing receptor Ffar2 (GPR43) in colonic ILC3 populations and delineate how Ffar2 signaling regulates ILC3 function.

INTRODUCTION

Innate lymphoid cells (ILC) play critical roles in immunity, tissue homeostasis and repair. ILCs are classified into three groups: Group 1 ILCs (ILC1s) require the transcription factor T-bet and produce interferon- γ (IFN-γ), Group 2 ILCs (ILC2s) express the transcription

factor GATA3 and produce the type 2 cytokines IL-5 and IL-13, and Group 3 ILCs (ILC3s) are a heterogeneous population that express the transcription factor RAR-related orphan receptor gamma t (RORγt) and have the ability to produce IL-22 and/or IL-17 (Colonna, 2018; Vivier et al., 2018).

ILC3s are enriched in the gut where they maintain homeostasis by orchestrating lymphoid tissue development, commensal bacterial containment, tissue repair, host defense and regulation of adaptive immunity (Artis and Spits, 2015; Sonnenberg and Hepworth, 2019). ILC3s can be divided into two subsets based on C-C chemokine receptor type 6 (CCR6) expression (Klose and Artis, 2016). Both $CCR6^+$ ILC3s and $CCR6^-$ ILC3s produce IL-22, and $CCR6^+$ ILC3s can produce IL-17 (Gladiator et al., 2013). $CCR6^-$ ILC3s can express NKp46, and $NKp46^+$ ILC3s express T-bet and can produce IFN-γ. $CCR6^-$ $NKp46^-$ ILC3s have the capacity to differentiate into $NKp46^+$ ILC3s (Klose et al., 2013). Beyond the heterogeneity between $CCR6^+$ and $CCR6^-$ ILC3s noted above, little is known about how the microbiota or microbial metabolites impact their diversity and function.

ILC3s process signals from other cells and soluble mediators within their tissue microenvironment (Withers and Hepworth, 2017), and environmental cues, e.g. microbial, dietary, and neuronal signals, regulate ILC3s through cell-intrinsic receptors. Bacterial metabolites and dietary components engage the aryl hydrocarbon receptor (Ahr) and promote ILC3 proliferation and cytokine secretion (Qiu et al., 2012). Retinoic acid (RA) and RA receptors (RARs) enhance IL-22 by ILC3s (Mielke et al., 2013). Glial-derived neurotropic factor family ligands (GFLs) also controls ILC3s via neuroregulatory receptor (RET) signaling (Ibiza et al., 2016).

Of the many bacterial metabolites in the gut (Rooks and Garrett, 2016), short-chain fatty acids (SCFAs) have emerged as critical regulators of immune responses (Erny et al., 2015; Perry et al., 2016). SCFAs, produced in the colon through bacterial fermentation of dietary fiber, engage ‘metabolite-sensing’ G-protein-coupled receptors (GPCRs) (Koh et al., 2016; Tan et al., 2017). Ffar2, also known as GPR43, is a SCFA-sensing GPCR that exerts immunomodulatory effects and functions in gut homeostasis and regulation of inflammation (Koh et al., 2016; Tan et al., 2017). Loss of Ffar2 in mice attenuates inflammation in colitis and arthritis models via altering leukocyte chemotaxis (Maslowski et al., 2009). Ffar2 also mediates colonic regulatory T (Treg) cell expansion and protects against T-cell transfer colitis (Smith et al., 2013). However, if Ffar2 signaling regulates colonic ILC3s remains unknown.

Herein, we show that colonic ILC3s express Ffar2 transcripts and Ffar2 agonism selectively promotes colonic ILC3 population and its function. Loss of *Ffar2* in ILC3s decreased colonic ILC3 *in situ* proliferation and ILC3-derived IL-22 production. Ffar2 agonism enhanced $CCR6^+$ ILC3 *in situ* proliferation, IL-22 production and accumulation in colonic lymphoid tissues. $Ffar2^{-/-}$ ILC3s had impaired gut epithelial function attributed to altered mucus-associated protein and antimicrobial peptide expressions. Hence, mice that have $Ffar2^{-/-}$ ILC3s were more susceptible to colonic injury and infection. Furthermore, Ffar2 agonism differentially activated $G_{i/o}$ and G_q subunits and consequently AKT or ERK signaling downstream of Ffar2, leading to direct regulation of colonic ILC3-derived IL-22

via AKT and STAT3. Our results demonstrate that Ffar2 regulates colonic ILC3 proliferation and function and that Ffar2 signaling in ILC3s modulates gut inflammatory tone and pathogen defense.

RESULTS

Ffar2 agonism selectively promotes colonic ILC3 expansion and function

To investigate a role for Ffar2 in colonic ILCs, we profiled their *Ffar2* expression. Colonic ILCs highly expressed *Ffar2* compared to myeloid cells and granulocytes (Figure 1A). ILC2s and ILC3s abundantly expressed *Ffar2* transcripts compared to ILC1s (Figure 1B). *Ffar2* was also expressed in ILC2s and ILC3s of the small intestine (SI) (ileum) and mesenteric lymph nodes (MLN) (Figure 1B). Colonic ILC2s and ILC3s had lower *Ffar2* expression than ileal ILC2s and ILC3s. However, previous studies have shown that the concentration of SCFAs such as acetate(A), propionate(P) and butyrate(B), both in human and mice are higher in the cecum (proximal colon) versus the SI (e.g. in humans, a ratio of A, 8.7:1; P, 16.8:1; B11.8: 1 and in mice, a ratio of A, 2.7:1; P, 8.4:1; B, 2.6: 1) (Cummings et al., 1987; Smith et al., 2013). Given that the colon has higher luminal SCFA concentrations and ILCs are tissue-resident cells (Vivier et al., 2018), we focused on the role of Ffar2 in colonic ILC populations rather than SI. To examine how Ffar2 expression regulates colonic ILC2s and ILC3s, we began by feeding mice natural Ffar2 ligands, SCFAs, and analyzed both ILC populations. Acetate and to a lesser extent, propionate, increased colonic ILC3 frequency and number compared to control (NaCl), whereas neither altered colonic ILC2s (Figure 1C). In contrast to the role of butyrate in suppressing Peyer's patch (PP) ILC3s (Kim et al., 2017), neither colonic ILC2s nor ILC3s were affected by butyrate (Figure 1C). Given that IL-22 and/or IL-17 are key cytokines for ILC3 function (Artis and Spits, 2015; Spits and Cupedo, 2012); we examined if SCFAs regulate ILC3 cytokine production. Butyrate did not affect the population frequency or cell number of IL-22 or IL-17A producing ILC3s (Figure 1D). Propionate and to a lesser extent, acetate, increased IL-22$^+$ ILC3s compared to control while neither propionate nor acetate altered IL-17A$^+$ ILC3s (Figure 1D).

These differential effects of propionate and acetate versus butyrate that resulted in selective promotion of colonic ILC3 expansion and IL-22 production were consistent with the relative agonistic potency of each SCFA for Ffar2 (Le Poul et al., 2003).

As SCFAs can enter cells through membrane transporters and also affect cellular epigenetic changes as HDAC inhibitors (Tan et al., 2017), to more definitively elucidate a potential role for Ffar2 in ILCs, we employed a synthetic Ffar2 agonist. This agonist is specific for Ffar2 and induces Ffar2 signaling in nM concentrations, in contrast with SCFAs which have EC_{50}s in the μM range (Forbes et al., 2015; Hoveyda, 2011). The Ffar2 agonist increased both ILC3 frequency and cell number while colonic ILC2s slightly decreased in frequency but not in number (Figure 1E). These data led us to ask if Ffar2 agonism selectively decreases ILC2s or increases ILC3s. We analyzed the proliferation marker Ki-67 in both ILC2s and ILC3s. Colonic ILC2s exhibited limited Ki-67 expression and the Ffar2 agonist did not alter Ki-67-expressing ILC2 frequency (Figure 1F). In contrast, colonic ILC3s proliferated under steady state conditions and the Ffar2 agonist increased the frequency and number of Ki-67-

expressing ILC3s (Figure 1F). Previous studies have reported a low proliferation rate of ILC3s in the SI at steady state (Sawa et al., 2010; Withers et al., 2016). To further validate the proliferation rate of colonic ILC3s observed, we performed *in vivo* BrdU incorporation experiments in mice fed the synthetic Ffar2 agonist. Colonic ILC3s were rapidly proliferating and the Ffar2 agonist increased $BrdU^+$ ILC3 frequency and number (Figure 1G). The Ffar2 agonist also increased IL-22^+ ILC3 population frequency and number but did not significantly affect IL-13^+ ILC2 number (Figure 1H). These results support that a synthetic Ffar2 agonist selectively increases colonic ILC3 expansion and function similar to the effects observed with acetate and propionate.

Given that colonic myeloid cells and some T cell populations express Ffar2 transcripts, we examined if the synthetic Ffar2 agonist affected other colonic immune cells. The Ffar2 agonist did not change colonic myeloid cells ($CD11b^+$ cells, $CD11c^+$ $MHCII^+$ DCs, $CD103^+$ DCs and $CD11b^+$ Gr-1^+ cells) (Figure S1A) or T cell populations ($Tbet^+$ Th1, $GATA3^+$ T helper-2 (Th2), $ROR\gamma t^+$ Th17 and $Foxp3^+$ Treg cells) under our experimental conditions (Figure S1B).

ILC3s are regulated by cell-extrinsic factors, including: cytokines, growth factors and dietary metabolites (Withers and Hepworth, 2017). IL-23 produced by macrophages and DCs is a key regulator of ILC3 activation (Kinnebrew et al., 2012; Longman et al., 2014). We did not observe an effect of the Ffar2 agonist in colonic myeloid cell expansion in the same time frame over which ILC3s were affected (Figure S1B). However, to test if Ffar2 agonism can induce myeloid cell-derived IL-23 in the colon, we analyzed IL-23 expression in the colonic lamina propria from mice fed SCFAs or the synthetic Ffar2 agonist. Neither the Ffar2 agonist nor propionate affected IL-23 expression, whereas acetate increased IL-23 expression in the colonic lamina propria (Figures S1C and S1D), suggesting that both the synthetic Ffar2 agonist and propionate may regulate colonic ILC3s in a cell-intrinsic manner, but acetate may affect ILC3s additionally by bolstering cell-extrinsic IL-23 production.

Whether the microbiota affects ILC3 populations has remained controversial. Some studies suggest that germ-free (GF) mice exhibit a decrease in IL-22^+ $NKp46^+$ ILC3s (Satoh-Takayama et al., 2008), whereas other studies have shown that the microbiota functions as a negative regulator of ILC3s in the SI (Sawa et al., 2011). In our studies, both colonic ILC3s and IL-22^+ ILC3s decreased in GF mice compared to conventionally- housed, specific pathogen-free (SPF) WT mice (Figure 2A). To corroborate the role of Ffar2 agonism in colonic ILC3 expansion and function and rule-out that the effects observed stemmed from Ffar2 agonism affecting the microbiota directly, we fed GF mice acetate, propionate or the Ffar2 agonist. Consistent with our prior observations (Figures 1C and 1D), acetate increased ILC3 number and frequency (Figure 2B) while propionate increased IL-22^+ ILC3s (Figure 2C). The Ffar2 agonist increased both colonic ILC3s and IL-22^+ ILC3s in GF mice (Figure 2D). Collectively, these data suggest that Ffar2 agonism by natural Ffar2 ligands or a synthetic Ffar2 agonist selectively promotes colonic ILC3 expansion and function and that Ffar2 could be a positive regulator of colonic ILC3 expansion and ILC3-derived IL-22.

Ffar2 regulates colonic ILC3 proliferation and ILC3-derived IL-22 production

To confirm the role of Ffar2 in colonic ILC3s, we also analyzed colonic ILC3s in *Ffar2*$^{-/-}$ versus littermate control (LC) WT mice. The population frequencies and numbers of colonic ILC3s and IL-22^{+} ILC3s decreased in *Ffar2*$^{-/-}$ mice indicating that Ffar2 deficiency affects colonic ILC3 expansion and function (Figure 3A). To determine how Ffar2 deficiency influences colonic ILC3s at a global transcriptomic level, we performed RNA sequencing (RNA-seq) on sorted ILC3s from WT and *Ffar2*$^{-/-}$ mice. Signature gene expression such as the master transcription factor RORγt, ILC3 subset surface markers, e.g. CCR6 and NKp46, and IL-22, decreased in *Ffar2*$^{-/-}$ ILC3s while another master transcriptional factor, the aryl hydrocarbon receptor (Ahr), and IL-17a were similar in WT and *Ffar2*$^{-/-}$ ILC3s (Figure 3B). Flow cytometry analysis confirmed the decreased expression of RORγt, CCR6, NKp46 and IL-22 in *Ffar2*$^{-/-}$ vs. WT ILC3s (Figure 3C). We more broadly investigated gene signatures related to ILC3 transcriptional programs, cell surface markers, chemokines, cytokines and cellular molecules some of which have been previously reported on in ILC3s (Figure S2A) (Gury-BenAri et al., 2016; Robinette et al., 2015). Differential expression analysis revealed upregulated pathways involved in ILC3 cellular functions, anti-apoptotic process, and metabolic processes including lipid metabolism in WT ILC3s (Figure S2B). Consistent with a prior transcriptional profiling study which identified specific core metabolic functions in ILC3s (Di Luccia et al., 2019; Gury-BenAri et al., 2016), WT ILC3s showed increased expression of the glycolytic mediators (e.g. hexokinase and phosphofructokinase) and increased acyl-CoA dehydrogenase, ATP citrate lyase, fatty acid synthase, HMG-CoA synthase 1 and monoglyceride lipase, which are involved in lipogenesis and fatty acid metabolism (Figure S2C). In WT ILC3s, genes involved in anti-apoptotic processes and altered gene signatures associated with the cell cycle were also upregulated (Figures S2D and S2E). These data suggest that Ffar2 may influence the expression of a multitude of genes and pathways in ILC3 related to their maintenance, core cellular functions, and metabolism.

To decipher the cell-intrinsic role of Ffar2 in colonic ILC3s, we generated *Rorc-cre Ffar2*$^{fl/fl}$ mice that lack Ffar2 in RORγt^{+} ILC3s and T cells (referred to as *Ffar2*$^{\Delta Rorc}$ mice). ILC3 frequency and number decreased in *Ffar2*$^{\Delta Rorc}$ mice compared to *Ffar2*$^{fl/fl}$ mice (Figure 3D), whereas total ILCs were unaffected by Ffar2 ablation (Figure S2F). These data led us to determine if Ffar2 regulates RORγt^{+} ILC3 proliferation. Ki-67^{+} RORγt^{+} ILC3 decreased in *Ffar2*$^{\Delta Rorc}$ compared to *Ffar2*$^{fl/fl}$ mice (Figure 3E), whereas Ki-67 expression in GATA3^{+} ILC2s was not affected (Figure S2G). Consistently, the frequency and number of BrdU^{+} ILC3s decreased in the conditional KO mice (Figure 3F). We next examined if Ffar2 regulates IL-22 and/or IL-17A production in RORγt^{+} ILC3s. IL-22^{+} ILC3s decreased in *Ffar2*$^{\Delta Rorc}$ mice, whereas IL-17A^{+} ILC3s were not altered in *Ffar2*$^{\Delta Rorc}$ mice (Figure 3G). A subset of CD4^{+} T cells, T helper (Th) 17 cells, express RORγt and also produce IL-22 and/or IL-17 (Korn et al., 2009). In contrast to RORγt^{+} ILC3s, *Ffar2*$^{\Delta Rorc}$ mice did not show alterations in colonic RORγt^{+} CD4^{+} T cell frequency and number (Figure S2H). Neither IL-22 nor IL-17A production was affected in RORγt^{+} CD4^{+} T cells from *Ffar2*$^{\Delta Rorc}$ mice (Figure S2I). Additionally, other T cell populations including Foxp3^{+} Treg cells, Tbet^{+} Th1 cells, GATA3^{+} Th2 cells, and RORγt^{+} γδ T cells were not altered in *Ffar2*$^{\Delta Rorc}$ mice (Figures S2J and S2K). This observation was entirely consistent with earlier work from our

group wherein we did not observe changes in Foxp3$^+$ Tregs in *Ffar2*$^{-/-}$ mice under homeostatic conditions (Smith et al., 2013) and also supports that Ffar2 in ILC3s does not affect RORγt-expressing T cells.

To rule out any influence of adaptive immune responses more generally, we generated *Rag2*$^{-/-}$*Ffar2*$^{\Delta Rorc}$ mice and analyzed their colonic ILC2s and ILC3s. Consistent with our data in *Ffar2*$^{\Delta Rorc}$ mice, colonic ILC3s and IL-22$^+$ ILC3s decreased in *Rag2*$^{-/-}$*Ffar2*$^{\Delta Rorc}$ compared to *Rag2*$^{-/-}$*Ffar2*$^{fl/fl}$ mice (Figure 3H), whereas ILC2s and IL-13$^+$ ILC2s did not change in *Rag2*$^{-/-}$*Ffar2*$^{\Delta Rorc}$ mice (Figure S2L).

Given that ILC3s in the SI and MLN express Ffar2 transcripts (Figure 1B), we examined ILC3s in SIs, MLNs and PPs from *Ffar2*$^{\Delta Rorc}$ mice. The population frequency and numbers of SI (ileal) ILC3s did not change in *Ffar2*$^{\Delta Rorc}$ mice (Figure S2M). Neither IL-22$^+$ ILC3s nor IL-17$^+$ ILC3s changed in the SI of the conditional KO mice (Figure S2M). ILC3s and their functions (e.g., IL-22 and IL-17 production) in the MLNs and PPs did not change in *Ffar2*$^{\Delta Rorc}$ mice compared to controls (Figures S2N and S2O).

The transcription factors RORγt and Ahr are critical for ILC3 development and function (Eberl and Littman, 2004; Kiss et al., 2011). Consistent with our RNA-seq and flow cytometry analysis in WT and *Ffar2*$^{-/-}$ ILC3s (Figures 3B and 3C), RORγt expression (MFI) was reduced in ILC3s from *Ffar2*$^{\Delta Rorc}$ mice compared to *Ffar2*$^{fl/fl}$ mice (Figure 3I) while Ahr expression (MFI) was not affected in RORγt$^+$ ILC3s (Figure 3J), suggesting that Ffar2 signaling could target RORγt in colonic ILC3 expansion and function.

We also determined if a cell-extrinsic factor such as IL-23 influences the effects of Ffar2 in colonic ILC3 in *Ffar2*$^{\Delta Rorc}$ mice. We observed that *Ffar2*$^{\Delta Rorc}$ mice had similar colonic expression of *Il23* compared to *Ffar2*$^{fl/fl}$ mice (Figure S2P). Consistent with the transcriptional profiling analysis (Figure S2A), sorted colonic ILC3s from condition KO mice and controls showed similar *Il23r* expression (Figure S2Q). In addition to IL-23, IL-1β can activate ILC3-derived IL-22 (Cella et al., 2010). IL-1β expression did not differ in conditional KO mice versus controls (Figure S2R) and WT and *Ffar2*$^{-/-}$ colonic ILC3s showed similar *Il1r1* expression (Figure S2A), supporting that Ffar2's signaling role in ILC3 activation is likely independent of IL-23 or IL-1β signaling in *Ffar2*$^{\Delta Rorc}$ mice. Collectively, these data support that Ffar2 regulates colonic ILC3 proliferation and IL-22 production in a cell-intrinsic manner.

Ffar2 influences colonic CCR6$^+$ ILC3 expansion and function

Our observations that Ffar2 affects expression and frequency of CCR6 and NKp46 in colonic ILC3s (Figures 3B and 3C) and that two colonic ILC3 subsets, CCR6$^+$ ILC3s and CCR6$^-$ ILC3s, had different expression of Ffar2 transcripts (Figure S3A) led us to examine the role of Ffar2 in ILC3 subset functional diversity. CCR6$^+$ ILC3s decreased in conditional KOs compared to controls while CCR6$^-$ ILC3s including NKp46$^+$ ILC3s did not change in conditional KOs (Figure 4A). The CCR6$^+$ ILC3 population was a major ILC3 subset in the colon (Figure 4A) and the frequency and number of Ki-67$^+$ CCR6$^+$ ILC3s were much higher as compared to CCR6$^-$ and NKp46$^+$ ILC3s (Figure S3B). Both CCR6$^+$ and CCR6$^-$ ILC3s produce IL-22 (Klose and Artis, 2016). However, we found that the majority of CCR6$^+$

ILC3s were IL-22$^+$ cells in the colon, whereas CCR6$^-$ and NKp46$^+$ ILC3s showed relatively reduced IL-22 production (Figure 4B). Consistent with these findings in CCR6$^+$ ILC3s, IL-22$^+$ CCR6$^+$ ILC3s decreased in *Ffar2*$^{\Delta Rorc}$ mice while CCR6$^-$ and NKp46$^+$ ILC3s were not affected in the conditional KO mice (Figure 4B), supporting that Ffar2 expression may contribute to colonic CCR6$^+$ ILC3 abundance and function, e.g. IL-22 production.

Given the effects of Ffar2 expression on CCR6$^+$ ILC3s, which are localized in colonic lymphoid tissues (Baptista et al., 2013; Emgard et al., 2018), we examined if Ffar2 expression within ILC3s affects these structures. To analyze the distribution of colonic Ffar2-expressing ILC3s, we employed RNA *in situ* hybridization due to poor anti-Ffar2 antibody availability and quality for formalin-fixed paraffin embedded tissues and visualized *Ffar2*-expressing ILC3s in conjunction with antibodies staining to identify ILC3 in colonic tissue sections. Colonic RORγt$^+$ CD3$^-$ ILC3s clustered in the borders of colonic patches (CPs) and in colonic solitary intestinal lymphoid tissues (SILTs) in *Ffar2*$^{\Delta Rorc}$ and *Ffar2*$^{fl/fl}$ mice (Figures 4C). We confirmed the selective deletion of *Ffar2* in ILC3s from both CPs and SILTs in *Ffar2*$^{\Delta Rorc}$ compared to *Ffar2*$^{fl/fl}$ mice (Figures 4C) and observed that the number of *Ffar2*-expressing colonic ILC3s (*Ffar2*$^+$ RORγt$^+$ CD3$^-$) in CPs was higher than in SILTs (Figure 4D). To determine if Ffar2-expressing ILC3s influenced the development of colonic lymphoid structures, we counted the number of CPs and SILTs in *Ffar2*$^{\Delta Rorc}$ and *Ffar2*$^{fl/fl}$ mice and they did not differ (Figure 4E). In contrast, the number of RORγt$^+$ CD3$^-$ ILC3s within both CPs and SILTs decreased in *Ffar2*$^{\Delta Rorc}$ compared to *Ffar2*$^{fl/fl}$ mice (Figure 4F). These data support that Ffar2 influences CCR6$^+$ ILC3 subset expansion and function and that Ffar2-expressing ILC3s are not required for the development of colonic lymphoid tissues, but rather may contribute to ILC3 abundance in colonic lymphoid tissues.

Ffar2 expression in ILC3s affords protection from intestinal inflammation

IL-22-producing ILC3s play key roles in tissue homeostasis and host defense by regulating gut epithelial barrier functions such as mucus and antimicrobial peptide production (Rutz et al., 2013; Sanos et al., 2011; Sonnenberg et al., 2011). Analysis of targeted gut epithelial transcriptional signatures from *Ffar2*$^{\Delta Rorc}$ mice revealed decreased mucin (*Muc2*, *3*, *4*, and *5b*) and antimicrobial peptide (*Reg3α*, *β*, and *γ*) expression (Figure 5A) while gut permeability and bacterial translocation were not significantly affected in conditional KO mice under steady state condition (Figures S4A and S4B). Given the down-regulation of epithelial barrier transcriptional signatures and decreased IL-22$^+$ ILC3s (Figure 3F) in *Ffar2*$^{\Delta Rorc}$ mice, we investigated the role of Ffar2 in colonic host repair and defense. We employed a dextran sodium sulfate (DSS) colonic injury model and determined if Ffar2 expression in ILC3s contributes to the regulation of gut injury and inflammation. *Ffar2*$^{\Delta Rorc}$ mice treated with DSS showed increased weight loss (Figure 5B) and shortened colon length (Figure 5C). We also observed worse histological colitis scores (Figure 5D) and more severely inflamed colons in *Ffar2*$^{\Delta Rorc}$ compared to *Ffar2*$^{fl/fl}$ mice (Figure 5E). Notably, IL-22$^+$ ILC3s decreased in *Ffar2*$^{\Delta Rorc}$ mice treated with DSS compared to controls (Figure 5F). Consistent with our observations under steady state condition (Figure 4B); the majority of IL-22$^+$ ILC3s were CCR6$^+$ ILC3s, and IL-22$^+$ CCR6$^+$ ILC3s decreased in *Ffar2*$^{\Delta Rorc}$ mice treated with DSS (Figure 5G). Although the DSS perturbation increased RORγt$^+$ Th17 cells and specifically IL-17A$^+$ RORγt$^+$ Th17 cells compared to untreated *Ffar2*$^{\Delta Rorc}$ and

Ffar2$^{fl/fl}$ mice (Figures S4C and S2H), RORγt$^+$ Th17 cells including IL-22$^+$ and IL-17A$^+$ RORγt$^+$ Th17 cells did not change in *Ffar2*$^{\Delta Rorc}$ mice treated with DSS compared to conditional control mice (Figure S4C). Other T cell populations such as Foxp3$^+$ Treg cells, Tbet$^+$ Th1 cells, and GATA3$^+$ Th2 cells did not change in DSS-treated *Ffar2*$^{\Delta Rorc}$ and *Ffar2*$^{fl/fl}$ mice (Figure S4D). Expression of gut barrier signature genes such as *Muc4* and the antimicrobial peptides *Reg3α*, *β*, and *γ* decreased in *Ffar2*$^{\Delta Rorc}$ mice treated with DSS (Figure S4F), supporting that Ffar2 expression in ILC3s affords protection from colonic injury by regulating IL-22 production and consequently gut barrier function. To determine if the Ffar2 agonism can affect responses to a colonic injury-inflammatory perturbation, we fed WT mice with the Ffar2 agonist and then utilized the DSS model. The Ffar2 agonist treated mice had reduced body weight loss (Figure 5H), increased colon length ((Figure 5I) and decreased histological colitis scores compared to controls (Figure 5J).

To evaluate the effect of Ffar2 in host defense, we utilized the *C. rodentium* infection model where ILC3-drived IL-22 is required to clear bacteria during the first week of infection (Zheng et al., 2008). *Ffar2*$^{\Delta Rorc}$ mice infected with *C. rodentium* rapidly lost body weight (Figure 6A) and displayed shortened colon length (Figure 6B). In addition, *C. rodentium*-infected *Ffar2*$^{\Delta Rorc}$ mice showed worse histological colitis scores (Figure 6C) and increased mucosal hyperplasia and submucosal inflammation compared to *C. rodentium*-infected *Ffar2*$^{fl/fl}$ mice (Figure 6D). IL-22$^+$ ILC3s and IL-22$^+$ CCR6$^+$ ILC3s decreased in *Ffar2*$^{\Delta Rorc}$ mice compared to conditional control mice (Figures 6E and 6F). *C. rodentium*-infected mice had an increase in IL-17A$^+$ RORγt$^+$ Th17 cells (Figures S5A and S2I). However, RORγt$^+$ Th17 cells including IL-22$^+$ and IL-17A$^+$ Th17 cells and other T cell populations did not change in conditional KO mice compared to controls (Figures S5A and S5B). Gut barrier function gene expression signatures, specifically *Reg3α*, *β*, and *γ*, were also reduced in *Ffar2*$^{\Delta Rorc}$ mice infected with *C. rodentium* (Figure S5C). Furthermore, there was increased *C. rodentium* translocation to the spleen and liver in *Ffar2*$^{\Delta Rorc}$ compared to *Ffar2*$^{fl/fl}$ mice (Figure 6G), supporting that Ffar2 expression in ILC3s contributes to host defense against enteric bacterial infection. Next, we determined if Ffar2 agonism affects disease severity in *C. rodentium* infection model by feeding WT mice the Ffar2 agonist and infecting mice with *C. rodentium*. Similar to our observations with the DSS model, the Ffar2 agonist reduced disease severity including body weight change, colon length and histological colitis scores in the *C. rodentium* infection model (Figures 6H–6J). Collectively, these data demonstrate a clear role for Ffar2 in gut immunity via regulation of ILC3-derived IL-22 and consequently gut epithelial function.

Ffar2 regulates ILC3-derived IL-22 via AKT and STAT3 activation

To investigate the signaling downstream of Ffar2 underpinning ILC3-derived IL-22 production, we sorted colonic ILC3s and stimulated the cells *ex vivo* with acetate, propionate or the Ffar2 agonist. The Ffar2 agonist, and to a lesser extent propionate, increased *IL22* expression in sorted ILC3s while acetate did not alter *IL22* expression (Figure 7A). Our *in vitro* BrdU incorporation analysis showed that acetate increased the percentage of BrdU$^+$ ILC3s while propionate did not (Figure S6A), supporting that acetate regulates colonic ILC3 expansion but not ILC3-derived IL-22 production. Ffar2 can couple with $G_{i/o}$ and/or G_q proteins and Ffar2 activation can inhibit cAMP and/or stimulate Ca^{2+}

influx eliciting intracellular signaling that regulates numerous cell-specific functions (Brown et al., 2003; Le Poul et al., 2003; Nilsson et al., 2003). We employed a $G_{i/o}$ inhibitor (pertussis toxin, PTX) and a G_q inhibitor (YM-254890) to determine if distinctive forms of Ffar2 agonism examined herein differentially affect ILC3-derived IL-22 through direct involvement of Ffar2 downstream canonical signal pathways. Both PTX and YM-254890 abolished *IL22* expression in sorted ILC3s stimulated with the synthetic Ffar2 agonist (Figure 7B). However, these $G_{i/o}$ and G_q inhibitors, upon activation with propionate, decreased *IL22* transcripts to a lesser extent (Figure 7C). This suggests that the synthetic Ffar2 agonist is likely more efficient in $G_{i/o}$ and G_q subunit-mediated signaling of Ffar2 compared to propionate and that propionate may engage additional signaling pathways downstream of Ffar2. These findings are consistent with the differential affinities of these agonists for Ffar2. A phosphoprotein expression analysis suggested that Ffar2 agonism with SCFA activated MAP kinase pathways, PI3K-AKT, and PKC via $G_{i/o}$ or G_q proteins in neutrophils (Maslowski et al., 2009). To further evaluate how Ffar2 signaling regulates colonic ILC3-derived IL-22, we profiled protein phosphorylation of candidate Ffar2 downstream effectors by flow cytometry. *Ffar2*$^{-/-}$ ILC3s exhibited reduced percentage and MFI for phosphorylated AKT, p38, and ERK (Figures 7D and S6B). Given that STAT3 phosphorylation (pSTAT3) is a critical regulator for ILC3-derived IL-22 (Guo et al., 2014), we examined if Ffar2 signaling regulates STAT3 activation in colonic ILC3s. *Ffar2*$^{-/-}$ ILC3s showed a decreased percentage of pSTAT3$^+$ compared to WT ILC3s (Figures 7E and S6C). To evaluate if Ffar2 agonism activates these signaling molecules in colonic ILC3s, we stimulated sorted ILC3s with propionate or the synthetic Ffar2 agonist *ex vivo*. The synthetic Ffar2 agonist increased AKT and STAT3 phosphorylation, but not p38 and ERK in WT ILC3s (Figures 7F and S6D). As expected, treatment of *Ffar2*$^{-/-}$ ILC3s with the synthetic Ffar2 agonist had no effect on these signaling molecules (Figure S6E). In contrast, propionate did not induce phosphorylation of these molecules in WT ILC3s (Figure 7F). However, given that propionate has lower potency for Ffar2 compared to the synthetic Ffar2 agonist and that propionate is likely to induce ERK phosphorylation (Figure 7F), we examined if a longer treatment with propionate would activate ERK signaling in Ffar2-sufficient ILC3s. The longer stimulation (1hr vs 30min) did induce a higher ERK phosphorylation in sorted ILC3s, but the percentage of pERK$^+$ ILC3s was comparable to that observed with the shorter time (Figure S6F). Under these conditions, we also examined if the longer time with propionate led to pSTAT3 in ILC3s. Propionate did increase pSTAT3$^+$ ILC3s, but only 1–1.5% of the ILC3s were pSTAT3$^+$ (Figure S6G). Next, we tested if Ffar2 agonism-induced signaling pathways directly affect IL-22 expression in sorted ILC3s. We pretreated ILC3s with an AKT or an ERK inhibitor prior to stimulation with the Ffar2 agonist or propionate, respectively. The AKT inhibitor, upon Ffar2 activation with the synthetic Ffar2 agonist, decreased *Il22* expression in colonic ILC3s, similar to the STAT3 inhibitor (Figure 7G). In contrast, the ERK inhibitor prior to the longer propionate stimulation did not affect IL-22 expression in sorted ILC3s (Figure S6H). Also, inhibition of AKT, upon Ffar2 activation with the agonist, impaired STAT3 activation in ILC3s (Figure 7H), supporting that AKT activation downstream of Ffar2 may directly affect STAT3 phosphorylation in ILC3s. Collectively, these data support that Ffar2 agonism by the synthetic Ffar2 agonist or propionate differentially regulates colonic ILC3-derived IL-22 expression via AKT and STAT3 axis or partially via ERK and STAT3 activation.

DISCUSSION

Dietary and bacterial metabolites regulate immune responses and influence gut health. Some of these metabolites directly activate metabolite-sensing GPCRs and these engagements induce immunological responses that contribute to mucosal homeostasis and intestinal immunity. Our study unveiled a heretofore unknown role for Ffar2 in ILC3s and sheds light on several aspects of ILC3 biology ranging from the contested role of the microbiota in affecting ILC3 populations to the transcriptional networks and their inputs that control ILC3s.

We found that Ffar2 provided functional inputs for ILC3 transcriptional regulation. RORγt is critical for the regulation of ILC3 development and function (Eberl and Littman, 2004), and Notch and Ahr contribute to ILC3 development as well (Serafini et al., 2015). Our study proposes that Ffar2 is also a key regulator of ILC3 maintenance and function through modulating RORγt expression within ILC3s. We do not suggest that Ffar2 directly binds to *Rorc* or *Il22* UTRs like Ahr and ARNT complexes do (Lee et al., 2011); rather, signals downstream of Ffar2 mediate such effects. Ffar2 deficiency in ILC3s decreased AKT and MAP kinase (p38 and ERK1/2) activation and STAT3 phosphorylation (pSTAT3) restraining optimal IL-22 production requisite for gut epithelial barrier integrity and gut homeostasis. Ffar2 agonism triggered $G_{i/o}$ and G_q subunit-mediated signaling downstream of Ffar2 and induced distinct signaling pathways by which Ffar2 ligands engaged Ffar2 in ILC3s. Indeed, a synthetic Ffar2 agonist enhanced IL-22 through inducing AKT activation and increasing $pSTAT3^+$ ILC3s. In contrast, propionate, a physiologic ligand of Ffar2, activated ERK1/2 signaling and increased a small number of $pSTAT3^+$ ILC3s that was not sufficient to regulate ILC3-derived IL-22 expression in our experiments. We attribute the disparity in the effects of the synthetic Ffar2 agonist versus propionate to differential engagement of Gα subunits downstream of Ffar2 in ILC3s that resulted in different signal thresholds for ILC3 function. Although propionate and the synthetic Ffar2 agonist similarly increased ILC3-derived IL-22 *in vivo* and *in vitro*, the differences in signaling molecule activation downstream of Ffar2 suggest that propionate may engage additional pathways. Our previous work demonstrated that propionate reduces HDAC expression in Ffar2-sufficient Treg cells but not Ffar2-deficient Treg cells (Smith et al., 2013). Similarly, colonic ILC3s expressed HDAC gene family members and Ffar2 was involved in regulation of HDAC expressions in ILC3s as suggested by our RNA-seq analysis. Thus, propionate may regulate cellular responses (e.g. IL-22 production) by affecting epigenetic changes in ILC3s as an HDAC inhibitor. Such effects, while not examined in this study, may influence ILC3 function as has been observed for Treg cells (Arpaia et al., 2013; Furusawa et al., 2013).

Ffar2 is expressed in both colonic and SI ILC3s; however, we explored how Ffar2 regulated colonic ILC3 expansion and function. The SI and colon are distinct ecological, physiological and immunological niches composed of different environmental cues such as microbes, metabolites, nutrients and growth factors (Mowat and Agace, 2014). SCFAs are abundant in the colon as opposed to the SI whereas retinoic acid, a well-known regulator of ILC3 populations, is abundant in the SI. Our data support the importance of environmental inputs and the integration of such receptor signaling for ILC3 regulation as well as the import of Ffar2 agonism in regulating colonic ILC3s in a niche-specific manner.

ILC3 subsets share common functions but have transcriptionally and functionally distinct features in different tissue environments. We observed that $CCR6^+$ ILC3s constituted the majority of colonic ILC3s and these cells were more proliferative and activated (higher IL-22 production) as compared to $CCR6^-$ ILC3 and $NKp46^+$ ILC3s. We postulate that Ffar2 may affect the development of $CCR6^+$ ILC3 progenitor cells. Given that all colonic ILC subsets do not change in conditional KO versus control mice and *Id2*, an essential transcription factor for ILC development did not change; there seems to be no effect of Ffar2 on very early ILC3 progenitors. Ffar2 may regulate transcriptional factors such as Notch in conjunction with T-bet and TOX, which has been proposed to contribute to development of $NKp46^+$ ILC3s and LTi-like cells, respectively (Aliahmad et al., 2010; Rankin et al., 2013). Our transcriptional profiling revealed that Ffar2 differentially regulated early progenitor-associated genes in colonic ILC3; *Tox*, *Kit*, and *Notch* were upregulated and *Gata3* and T-bet (*Tbx21*) were downregulated. Thus, further analysis of transcriptional networks of progenitors within the different lineage states would be needed to delineate the role of Ffar2 in the development and differentiation of colonic $CCR6^+$ ILC3s. Our data also suggest that Ffar2 may regulate apoptotic or survival factors for colonic $CCR6^+$ ILC3 expansion. Further investigation of how Ffar2 affects the expression of anti-apoptotic or cell survival factors in colonic $CCR6^+$ ILC3 expansion and function may provide insight into the role of Ffar2 regulation in colonic ILC3 subset diversity. Notably, we observed that Ffar2 affected colonic ILC3 abundance in lymphoid structures while Ffar2 is not likely required for lymphoid tissue formation. If Ffar2 is required for ILC3 recruitment to colonic lymphoid structures or if Ffar2 mainly accelerates $CCR6^+$ ILC3 proliferation after the localization to colonic lymphoid tissues merits further investigation.

In summary, our findings expand understanding of microbial metabolite-sensing receptors as critical regulators of ILC3 biology and ILC3-mediated mucosal immunity and elucidate the relevance of these signal thresholds for ILC3 function and ILC3 subset heterogeneity. Our study raises the question if manipulating Ffar2 signaling thresholds modulates the plasticity of ILC3s, discriminates redundant or non-redundant ILC3 subset function in different tissue microenvironments, and regulates the onset or progression of intestinal injury and inflammation through fine-tuning of ILC3 responses. Ffar2 signaling appears to play a pivotal role in ILC3s, differentially coordinating interactions with adaptive immune cells or gut epithelial components and shaping ILC3-mediated gut immunity. Elucidation of the molecular links between the Ffar2 and ILC3 responses may lead to reconsideration and repositioning of Ffar2 as therapeutic target for treatment of intestinal diseases including inflammatory bowel disease.

STAR METHODS

CONTACT FOR REAGENTS AND RESOURCE SHARING

Further information request for resources and reagents should be directed to the Lead Contact, Wendy Garrett (wgarrett@hsph.harvard.edu).

Mice—C57BL/6J (wild-type) mice were bred in-house and originally purchased from Jackson Laboratory. *Rorc-cre* mice (Eberl and Littman, 2004) on a C57BL/6J background

were originally generated in the laboratory of Dan Littman and purchased from Jackson Laboratory. *Ffar2* $^{fl/fl}$ mice on a C57BL/6J background were generously provided by Dr. Brian Layden (University of Illinois) and crossed with *Rorc-cre* mice to generate *Rorc-cre* x *Ffar2* $^{fl/fl}$ mice. *Ffar2* $^{-/-}$ mice on C57BL/6J background were obtained from UTSW and bred in-house. *Rag2* $^{-/-}$ mice were purchased from Jackson Laboratory crossed with *Rorc-cre* mice or *Ffar2* $^{fl/fl}$ mice to generate *Rag2* $^{-/-}$ *Rorc-cre* mice and *Rag2* $^{-/-}$ *Ffar2* $^{fl/fl}$ mice which are sequentially crossed to generate *Rag2* $^{-/-}$ *Rorc-cre* x *Ffar2* $^{fl/fl}$ mice. Germ-free animals were bred and maintained in semi-rigid gnotobiotic isolators under a strict 12-hour light cycle in the Harvard T. H. Chan Gnotobiotic Center for Mechanistic Microbiome Studies. Littermate controls were used and animals were cohoused after weaning. Male and female mice were used at 7–12 weeks of age. In individual experiments, all animals were age and sex-matched; exact numbers of animal used per experiment are indicated in figure legends. All mice were housed in microisolator cages in the barrier facility of Harvard T.H. Chan School of Public Health. Animal studies and experiments were approved and carried out in accordance with Harvard Medical School's Standing Committee on Animals and the National Institutes of Health guidelines for animal use and care.

Ffar2 agonist—Ffar2 agonist (compound 1 in patent no. WO 2011/076732 A1) was discovered and generously provided by Hamid Hoveyda and Graeme Fraser under Material Transfer Agreement permitting use of the compound (EPICS SA, Belgium) (Forbes et al., 2015; Hoveyda, 2011). This agonist has similar pharmacological activity at human and mouse receptor orthologs. Mice received 50mg/kg/d of Ffar2 agonist dissolved in distilled water (5ml/kg) provided by gentle oral administration twice a day for 1–2 weeks or the indicated duration. Germ-free (GF) mice were treated for 1–2 weeks with the Ffar2 agonist (700 μM) dissolved in autoclaved drinking water and filtered sterilized.

SCFA intervention—WT mice were treated for 2 weeks with sodium acetate (150mM) (S8750, Sigma), sodium propionate (150mM) (P5436, Sigma), or sodium butyrate (100mM) (303410, Sigma) dissolved in their autoclaved drinking water and filtered sterilized (Smith et al., 2013). WT control mice received sodium chloride (150mM). For GF mice, mice were treated for 2 weeks with sodium acetate (150mM), sodium propionate (150mM), or sodium chloride (150mM) as a control in the drinking water and filtered sterilized. Drinking water solutions were freshly prepared and changed every 5 days.

Isolation of colonic epithelial cells, immune cells from colonic and small intestinal lamina propria, MLNs and Peyer's patches—Colons were dissected and fat and blood vessels were removed. Colons were cut open longitudinally and washed with PBS to remove feces and debris, then incubated in PBS containing 5 mM EDTA, 0.145 mg/ml dithiothreitol (Sigma-Aldrich), 3% FBS and 1% penicillin/streptomycin (P/S) for 15 min at 37°C for 2 cycles. After being vortexed for 15s, the dissociated cells were collected as colonic epithelial cells. For the isolation of lamina propria immune cells, the remaining colonic tissues were washed twice in PBS, cut into 1mm in length, and digested in RPMI 1640 containing 0.5 mg/ml collagenase D (Roche), 0.01 mg/ml DNase I (Roche), and 0.5mg/ml dispase (Stem Cell Technologies) for 30 min at 37°C on a shaking platform. The digested tissues were passed through 70 μm strainers after being vigorously vortexed for

15s. Then, colonic immune cells were collected and resuspended in staining buffer (PBS with 1% fetal bovine serum and 1% penicillin-streptomycin solution (Corning)) for flow cytometry analysis, FACSAria sorting or RNA extraction. For isolation of small intestinal immune cells, the distal 10 cm of small intestine (ileum) was collected and epithelial cells were removed as detailed above. The remaining ileal tissues were minced into approximately 1 mm sections and digested in RPMI 10%FBS, 0.25mg/ml collagenase A (Roche), 50 μg/ml DNase (Roche), 0.1 units/ml Dispase (Stem Cell Technologies) for 25 min followed by a second digestion for 40 min. The digested tissues were passed through 40 μm strainers and ileal immune cells were collected. For isolation of immune cells from MLNs and Peyer's patches, MLNs and Peyer's patches were carefully removed and crushed through 40 μm strainers and resuspended in staining buffer or PBS.

Flow cytometry—Single-cell suspensions were stained with a combination of fluorescently conjugated monoclonal antibodies. CD16/32 antibody (93; BioLegend) was used to block the non-specific binding to Fc receptors before surface staining. Cells were stained with Fixable yellow dead cell stain kit (Invitrogen) for the detection of live/dead cells before staining of the cell surface. All antibodies were purchased from BioLegend unless otherwise specified. For surface marker staining, we used antibodies to the following mouse proteins: CD45 (30-F11), CD90.2 (53–2.1), lineage markers (17A2/RB6–8C5/RA3–6B2/Ter-119/M1/70), CCR6 (29–21.17), NKp46 (29A1.4), CD11b (M1/70), CD11c (N418), CD103 (2E7, eBioscience), Gr-1 (RB6–8C5), MHC class II (M5/114.15.2), NK1.1 (PK136), KLRG1 (2F1), CD3ε (145–2C11), CD4 (GK1.5), TCR gammadelta (GL-3, eBioscience).

For measurement of intracellular cytokine expression, cells were isolated *ex vivo* and stimulated with 50 ng/ml phorbol-12-myristate 13-acetate (PMA, Sigma-Aldrich) and 500 ng/ml ionomycin (Sigma-Aldrich) and Brefeldin (1000x solution, BioLegend) for 4 hr. Cells were subsequently surface-stained with a combination of the antibodies listed above, fixed and permeabilized using Foxp3 Fix/Perm Buffer set (BioLegend), and stained with IL-22-PerCP eFluor710 (1H8PWSR, eBioscience), IL-17A-Alexa Fluor 488 (eBio17B7, eBioscience),and IL-13-eFluor 660 (eBio13A, eBioscience).

For transcription factor expression, cell were isolated directly *ex vivo*, stained with antibodies to surface antigens, fixed and permeabilized according to the manufacturer's instructions (Foxp3 Fix/Perm Buffer set, BioLegend) and stained with phycoerythrin (PE) or Allophycocyanin (APC)-conjugated RORγt (B2D, eBioscience), Alexa Fluor 488-conjugated GATA3 (L50–823, BD Biosciences), eFluor 660-conjugated Ahr (4MEJJ, eBioscience), PerCP/Cyanine5.5-conjugated T-bet (4B10), PE-conjugated Foxp3 (FJK-16s, eBioscience), and PerCP eFluor710-conjugated Ki-67 (SolA15, eBiosciences).

For analysis of intracellular signaling in ILC3s (Ibiza et al., 2016), sorted colonic ILC3s were rested for 2 hr in RPMI at 37°C. Cells were unstimulated or stimulated with the Ffar2 agonist (10 μM dissolved in water, pH 7.4) or propionate (10 mM) for 30 min or 1hr at 37°C, fixed and permeabilized according to the manufacturer's instructions (BD Cytofix and BD Phosflow Perm Buffer III, BD Biosciences), and stained with Alexa Fluor 647-conjugated anti-AKT (pS473) (D9E, Cell Signaling Technology), anti-p38 MAPK (pT180/pY182) (36/038, BD Biosciences), anti-pERK1/2 (pT202/pY204) (E10, Cell Signaling

Technology) or anti-STAT3 (pY705) (4/p-STAT3, BD Biosciences) for 30 min at room temperature.

Cells were stained in parallel with the respective control isotype antibodies. FMO controls were performed as well. Stained cells were acquired on a BD LSRII flow cytometry (BD Biosciences) and analyzed with FlowJo9 software (Tree Star).

For sorting immune cells, colonic lamina propria immune cells, MLN cells, or splenocytes were obtained from 5–7 mice per one sorting session and sorted to > 95% purity using a FACSAria IIu at the Dana-Farber Cancer Institute Flow Cytometry Core. For sorting experiments, colonic immune cell populations and ILCs were identified as live $CD45^+NK1.1^+$ (conventional NK cell), $CD45^+CD11b^+Gr\text{-}1^+$ (granulocyte), $CD45^+CD11b^+Gr\text{-}1^-CD11c^-$ (macrophage), $CD45^+CD11c^+MHCII^+$ (conventional dendritic cell), $CD45^+Lin^-CD90.2^+$ (ILC),$CD45^+Lin^-$ $CD90.2^+$ $NK1.1^-$ $NKp46^+$ (ILC1), $CD45^+Lin^-$ $CD90.2^+$ $NK1.1^-$ $NKp46^{+/-}$ $KLRG1^+$ (ILC2), $CD45^+Lin^-$ $CD90.2^+$ $NK1.1^-$ $NKp46^{+/-}$ $KLRG1^-$ (ILC3), $CD45^+Lin^-$ $CD90.2^+$ $NK1.1^-NKp46^-$ $KLRG1^-CCR6^+$ ($CCR6^+$ ILC3s) and $CD45^+Lin^-$ $CD90.2^+$ $NK1.1^-NKp46^{+/-}$ $KLRG1^-CCR6^-$ ($CCR6^-$ ILC3s). The gating strategy for flow cytometry analysis and sorting experiments is provided in Figure S7.

***In vivo* BrdU incorporation—**Bromodeoxyuridine (BrdU) was dissolved at 10 mg/ml in PBS. 1mg of BrdU was administrated by intraperitoneal injection per mouse. After 18 h, colonic lamina propria immune cells were harvested and incorporation of BrdU was detected with the APC BrdU Flow Kit (BD Bioscience) according to the manufacturer's instructions.

RNA isolation and real-time quantitative PCR (qRT-PCR)—For analysis of sorted colonic immune cell populations including ILC subsets and colonic ILC3s, RNA was isolated using the RNeasy Micro Kit (Qiagen) or RNeasy Mini Kit (Qiagen) according to the manufacturer's protocol. For analysis of colonic epithelial cells or colon tissues, cells or tissues were homogenized directly into QIAzol (Qiagen), and RNA was isolated via chloroform extraction. The quantity and quality of RNA was determined using a NanoDrop (Thermo Scientific). For both methods, cDNA was synthesized with iScript Reverse Transcription Supermix for RT-qPCR (Bio-Rad). Quantitative real-time PCR was carried out on cDNA with SYBR FAST Universal qPCR Master Mix (KAPA Biosystems). Reactions were run on a Stratagene Mx3005P machine (Agilent Technologies). The expression of individual genes was normalized to housekeeping gene β-actin expression on the base of the ΔΔCt algorithm. Some results are shown as a fold induction relative to expression in colonic epithelial cells as indicated. Primer sequences are listed in Table S1. For analysis of universal 16S qPCR quantification in MLN, DNA was isolated using a standard phenol:chloroform extraction from MLNs and 80 ng of MLN DNA was analyzed using the following 16S universal primers as described (Nadkarni et al., 2002): forward, 5'-TCCTACGGGAGGCAGCAGT-3', reverse, 5'-GGACTACCAGGGTATCTAATCCTGTT-3'. 16S rRNA gene amplicon expression was normalized to housekeeping gene β-actin expression.

RNA-sequencing (RNA-seq)—Colonic ILC3s ($CD45^+Lin^-$ $CD90.2^+$ $NK1.1^-$ $NKp46^{+/-}$ $KLRG1^-$) were sorted from *Ffar2*$^{-/-}$ mice and littermate control WT mice. Two independent

RNA-seq experiments were performed. (i.e. two biological replicates (sex-matched) for each group that contained RNA from pooled colonic ILC3s from 10 to 15 mice). Sorted ILC3s were collected in RNAlater (Sigma-Aldrich) and RNA was extracted with RNeasy Micro Kit (Qiagen). RNA quality verification, library preparation, and sequencing were performed at BPF Next-Gen Sequencing Core Facility at Harvard Medical School. RNA samples showed an average 9.0 of RNA integrity number (RIN) and libraries were generated using SMART-seq v4 Ultra Low Input RNA kit (Takara Bio Inc.). Barcoded samples were pooled and sequenced over 4 lanes on a NextSeq 500 instrument (Illumina) to produce 75bp paired-end reads. Raw sequencing reads were demultiplexed and the adopter were trimmed by using Illumina's bcl2fastq2 Conversion software. Duplicate reads were removed based on Unique Molecular Identifier (UMI) base. Low quality reads were filtered by using sickle version 1.33 (https://github.com/najoshi/sickle). Reads were aligned to the NCBI GRCm38/mm10 mouse genome using the STAR aligner version 2.7 (Dobin et al., 2013) and filtered for uniquely mapped reads. Reads per gene were counted using HTSeq version 0.11.1(Anders et al., 2015). Differential expression was assessed by DESeq2 version 1.24.0 (Love et al., 2014) with default parameter. For pathway analysis (KEGG analysis), differentially expressed genes (2-fold difference and FPKM >=2) were used and analyzed by DAVID (Huang et al., 2007). Annotated gene ontology (GO) biological process was assigned to genes which were potentiated in ILC3s. Heatmapping were performed in R with pheatmap package version 1.0.12.

Histology—Colons were cleaned with PBS prior to fixation in 4% PFA and then processed by routine paraffin embedding, sectioning and H&E staining. Colitis scores were determined by a pathologist (J.N.G.), who was blinded to the experimental parameters. Each of the four histologic parameters was scored as absent (0), mild (1), moderate (2), or severe (3): mononuclear cell infiltration, polymorphonuclear cell infiltration, epithelial hyperplasia, and epithelial injury. The scores for the parameters were summed to generate the cumulative histologic colitis score as previously described(Garrett et al., 2007; Garrett et al., 2009). For the DSS-induced colonic injury model, cumulative histologic scores were also quantified as to the percentage involvement by the disease process: (1) <10%; (2) 10–25%; (3) 30–50%; (4) >50% and presented as histologic colitis scores (Dieleman et al., 1998) as follows: cumulative score * % involvement.

RNA *in situ* hybridization and immunofluorescence staining—To detect Ffar2-expressing RORγt$^+$ CD3$^-$ ILC3s in the colon, we performed RNA *in situ* hybridization, then subsequently carried out immunofluorescence staining. Mouse colon tissues were fixed overnight in 10% neutral buffered formalin (NBF) followed by routine paraffin embedding and sectioning. RNA *in situ* hybridization was performed using the Advanced Cell Diagnostic RNAscope Multiplex Fluorescent Detection Kit v2 (323100, ACDBio) according to the manufacturer's instructions (Wang et al., 2012). In brief, colon sections were deparaffinized, pretreated with Target Retrieval Reagents and protease, hybridized with Mm-Ffar2 probe (433711, ACDBio), and then underwent amplification steps. The chromogenic substrate TSA cyanine 3 (NEL744E001KT, PerkinElmer) was used to detect the *Ffar2* probe. Prior to DAPI counterstaining, immunofluorescence staining was performed following the Advanced Cell Diagnostic general recommendations (323100-TN). Briefly,

the samples were blocked in Tris-buffered saline (TBS) 1% BSA, 5% donkey serum and 5% goat serum for 1hr at room temperature, then incubated with anti-CD3 (rabbit polyclonal, 5690, Abcam) and anti-RORγt (rat monoclonal, 14-6988-80, eBioscience) primary antibodies overnight at 4°C. The sections were incubated for 1.5 hr at room temperature with a goat anti-rat-HRP (A10549, Invitrogen) secondary antibody and TSA cyanine 5 (NEL745E001KT, PerkinElmer) was used to detect RORγt positive cells. After an HRP blocking step, the sections were incubated for 1.5 hr at room temperature with a donkey anti-rabbit-HRP secondary antibody (711-035-152, Jackson ImmunoResearch) and CD3 positive cells were detected using TSA Fluorescein reagent (NEL741E001KT, PerkinElmer). The slides were counterstained with DAPI and mounted with Prolong Gold antifade mounting medium (P36934, Life Technologies). Images were acquired on a Nikon Eclipse NI-U equipped with a 20x, a 40x or a 60x objective or Nikon Eclipse Ti laser scanning microscope coupled with a 100x objective. Image analysis was performed using ImageJ. The numbers of colonic patches and SILTs were counted in whole colon tissue sections. For quantification of colonic ILC3s or *Ffar2*$^{+}$ ILC3s in the colonic tissues, 10 digital images of colonic patches and 26 images of colonic SILTs were selected. The number of RORγt^{+} CD3^{-} ILC3 number per each lymphoid tissue was counted by subtracting the number of RORγt^{+} CD3^{+} double positive cells from that of RORγt^{+} cells with DAPI-positive signals. Then *Ffar2*$^{+}$ ILC3s was selectively counted from RORγt^{+} CD3^{-} ILC3s per each lymphoid tissue. M.M. or E.C. performed quantification and was blinded to sample experimental identity.

FITC dextran feeding—Mice were gavaged with 4kDa FITC dextran (Sigma-Aldrich) (10mg/20g mouse, 10mg/100ul in sterile PBS). Mice had access to food and water *ad libitum* throughout. After 3hrs, blood was collected into serum separator tubes. Blood was spun for 5min at 5000rpm. Serum fluorescence intensities were measured (serum samples diluted 1:1 with PBS) with 485nm excitation and 528nm emission wavelength in a microplate reader (Molecular Devices).

DSS-induced colonic injury and inflammation model—*Rorc-cre Ffar2* $^{fl/fl}$ mice, *Ffar2* $^{fl/fl}$ mice or WT mice were treated with 3% (w/v) DSS (MP Biomedicals) *ad libitum* in the drinking water for 5 days and followed by regular drinking water for 2 days. Body weight was measured every day or every two days and mice were euthanized at day 7. Colon length was measured. Colon was fixed with 4% paraformaldehyde for histology or used for the isolation of colonic immune cells or colonic epithelial cells as describe above.

Citrobacter rodentium* infection model—Citrobater rodentium* (DBS100 strain) was generously provided by Dr. John Leong (Tufts University School of Medicine). *Rorc-cre Ffar2* $^{fl/fl}$ mice, *Ffar2* $^{fl/fl}$ mice or WT mice were orally infected with 4×10^{9} CFU of *C. rodentium* (Crepin et al., 2016). Mice were weighed daily or every two days. On day 7 after infection, the colon, spleen or liver were collected from the infected mice. Colon length was measured. Colon was fixed with 4% paraformaldehyde for histology or used for the isolation of colonic immune cells or colonic epithelial cells as describe above. For assessment of bacterial translocation (Bhinder et al., 2013), spleen and liver were weighed and

homogenized with a TissueRuptor (Qiagen). The homogenates were plated on MacConkey agar plate and counted after overnight incubation at 37°C under aerobic conditions.

***In vitro* BrdU incorporation—**Sorted ILC3s were cultured with BrdU (10 μM) during overnight stimulation with acetate and propionate and BrdU incorporation was detected with APC BrdU Flow Kit (BD Bioscience) according to the manufacturer's instructions.

$G_{i/o}$ and G_q inhibition—Sorted colonic ILC3s were rested for 2 hr in RPMI at 37°C. To determine *Il22* expression, cells were incubated with 500 ng/ml $G_{i/o}$ inhibitor (pertussis toxin, PTX, Calbiochem), 1 μM G_q inhibitor (YM-254890, Focus Biomolecues), or vehicle (sodium phosphate buffer or DMSO) as a control during overnight stimulation with the Ffa2 agonist or propionate at 37°C.

AKT, ERK and STAT3 inhibition—Sorted colonic ILC3s were rested for 2 hr in RPMI at 37°C. For analysis of STAT3 phosphorylation, cells were incubated with 10 μM AKT inhibitor VIII (VIII, Sigma-Aldrich)(Ibiza et al., 2016) or vehicle (DMSO) as a control for 1hr at 37°C before stimulation with the Ffar2 agonist (10 μM dissolved in water, pH 7.4). To determine *Il22* expression, cells were incubated with 10 μM AKT inhibitor VIII, 10 μM EKR inhibitor PD98059 (Ibiza et al., 2016), 10 μM STAT3 inhibitor VI (S3I, Sigma-Aldrich)(Ibiza et al., 2016) or vehicle during overnight stimulation with the Ffar2 agonist or propionate at 37°C.

Statistics—Data were analyzed with GraphPad Prism (version 7.0b). Data are shown as mean ± s.e.m as noted. For comparison between two independent experimental groups, an unpaired two-tailed Student's *t*-test when data were normally distributed or a two-tailed Mann-Whitney U test was used. For comparison between more than two groups, one-way ANOVA followed by Tukey's test or by Dunnett's test was performed. No samples were excluded from any experiments performed in this study. Mice were randomized to experimental groups on weaning or 1 wk prior to the start of an experimental intervention to avoid caged-based or housing bias. No blinding was used except for assignment of histologic scores and microscopy-based counting as noted above. Differences of $P < 0.05$ were considered statistically significant.

DATA AND SOFTWARE AVAILABILITY

The RNA sequencing data have been deposited in the NCBI Gene Expression Omnibus (GEO; https://www.ncbi.nlm.nih.gov/geo/) under accession number GEO: GSE137508.

Supplementary Material

Refer to Web version on PubMed Central for supplementary material.

ACKNOWLEDGEMENTS

This work is supported by NIH grant R01CA154426. B.T.L. is supported by NIH grant R01-DK104927 and Department of Veterans Affairs merit award I01-BX003382. We thank the BPF Next-Gen Sequencing Core Facility at Harvard Medical School. We thank L. Ricci for preparing the graphical abstract. We thank the Garrett Laboratory for helpful discussions and manuscript review.

REFERENCES

Aliahmad P, de la Torre B, and Kaye J (2010). Shared dependence on the DNA-binding factor TOX for the development of lymphoid tissue-inducer cell and NK cell lineages. Nat Immunol 11, 945–952. [PubMed: 20818394]

Anders S, Pyl PT, and Huber W (2015). HTSeq--a Python framework to work with high-throughput sequencing data. Bioinformatics 31, 166–169. [PubMed: 25260700]

Arpaia N, Campbell C, Fan X, Dikiy S, van der Veeken J, deRoos P, Liu H, Cross JR, Pfeffer K, Coffer PJ, and Rudensky AY (2013). Metabolites produced by commensal bacteria promote peripheral regulatory T-cell generation. Nature 504, 451–455. [PubMed: 24226773]

Artis D, and Spits H (2015). The biology of innate lymphoid cells. Nature 517, 293–301. [PubMed: 25592534]

Baptista AP, Olivier BJ, Goverse G, Greuter M, Knippenberg M, Kusser K, Domingues RG, Veiga-Fernandes H, Luster AD, Lugering A, et al. (2013). Colonic patch and colonic SILT development are independent and differentially regulated events. Mucosal Immunol 6, 511–521. [PubMed: 22990625]

Bhinder G, Sham HP, Chan JM, Morampudi V, Jacobson K, and Vallance BA (2013). The Citrobacter rodentium mouse model: studying pathogen and host contributions to infectious colitis. J Vis Exp, e50222. [PubMed: 23462619]

Brown AJ, Goldsworthy SM, Barnes AA, Eilert MM, Tcheang L, Daniels D, Muir AI, Wigglesworth MJ, Kinghorn I, Fraser NJ, et al. (2003). The Orphan G protein-coupled receptors GPR41 and GPR43 are activated by propionate and other short chain carboxylic acids. J Biol Chem 278, 11312–11319. [PubMed: 12496283]

Cella M, Otero K, and Colonna M (2010). Expansion of human NK-22 cells with IL-7, IL-2, and IL-1beta reveals intrinsic functional plasticity. Proc Natl Acad Sci U S A 107, 10961–10966. [PubMed: 20534450]

Colonna M (2018). Innate Lymphoid Cells: Diversity, Plasticity, and Unique Functions in Immunity. Immunity 48, 1104–1117. [PubMed: 29924976]

Crepin VF, Collins JW, Habibzay M, and Frankel G (2016). Citrobacter rodentium mouse model of bacterial infection. Nat Protoc 11, 1851–1876. [PubMed: 27606775]

Cummings JH, Pomare EW, Branch WJ, Naylor CP, and Macfarlane GT (1987). Short chain fatty acids in human large intestine, portal, hepatic and venous blood. Gut 28, 1221–1227. [PubMed: 3678950]

Di Luccia B, Gilfillan S, Cella M, Colonna M, and Huang SC (2019). ILC3s integrate glycolysis and mitochondrial production of reactive oxygen species to fulfill activation demands. J Exp Med.

Dieleman LA, Palmen MJ, Akol H, Bloemena E, Pena AS, Meuwissen SG, and Van Rees EP (1998). Chronic experimental colitis induced by dextran sulphate sodium (DSS) is characterized by Th1 and Th2 cytokines. Clin Exp Immunol 114, 385–391. [PubMed: 9844047]

Dobin A, Davis CA, Schlesinger F, Drenkow J, Zaleski C, Jha S, Batut P, Chaisson M, and Gingeras TR (2013). STAR: ultrafast universal RNA-seq aligner. Bioinformatics 29, 15–21. [PubMed: 23104886]

Eberl G, and Littman DR (2004). Thymic origin of intestinal alphabeta T cells revealed by fate mapping of RORgammat+ cells. Science 305, 248–251. [PubMed: 15247480]

Emgard J, Kammoun H, Garcia-Cassani B, Chesne J, Parigi SM, Jacob JM, Cheng HW, Evren E, Das S, Czarnewski P, et al. (2018). Oxysterol Sensing through the Receptor GPR183 Promotes the Lymphoid-Tissue-Inducing Function of Innate Lymphoid Cells and Colonic Inflammation. Immunity 48, 120–132 e128. [PubMed: 29343433]

Erny D, Hrabe de Angelis AL, Jaitin D, Wieghofer P, Staszewski O, David E, Keren-Shaul H, Mahlakoiv T, Jakobshagen K, Buch T, et al. (2015). Host microbiota constantly control maturation and function of microglia in the CNS. Nat Neurosci 18, 965–977. [PubMed: 26030851]

Forbes S, Stafford S, Coope G, Heffron H, Real K, Newman R, Davenport R, Barnes M, Grosse J, and Cox H (2015). Selective FFA2 Agonism Appears to Act via Intestinal PYY to Reduce Transit and Food Intake but Does Not Improve Glucose Tolerance in Mouse Models. Diabetes 64, 3763–3771. [PubMed: 26239054]

Furusawa Y, Obata Y, Fukuda S, Endo TA, Nakato G, Takahashi D, Nakanishi Y, Uetake C, Kato K, Kato T, et al. (2013). Commensal microbe-derived butyrate induces the differentiation of colonic regulatory T cells. Nature 504, 446–450. [PubMed: 24226770]

Garrett WS, Lord GM, Punit S, Lugo-Villarino G, Mazmanian SK, Ito S, Glickman JN, and Glimcher LH (2007). Communicable ulcerative colitis induced by T-bet deficiency in the innate immune system. Cell 131, 33–45. [PubMed: 17923086]

Garrett WS, Punit S, Gallini CA, Michaud M, Zhang D, Sigrist KS, Lord GM, Glickman JN, and Glimcher LH (2009). Colitis-associated colorectal cancer driven by T-bet deficiency in dendritic cells. Cancer Cell 16, 208–219. [PubMed: 19732721]

Gladiator A, Wangler N, Trautwein-Weidner K, and LeibundGut-Landmann S (2013). Cutting edge: IL-17-secreting innate lymphoid cells are essential for host defense against fungal infection. J Immunol 190, 521–525. [PubMed: 23255360]

Guo X, Qiu J, Tu T, Yang X, Deng L, Anders RA, Zhou L, and Fu YX (2014). Induction of innate lymphoid cell-derived interleukin-22 by the transcription factor STAT3 mediates protection against intestinal infection. Immunity 40, 25–39. [PubMed: 24412612]

Gury-BenAri M, Thaiss CA, Serafini N, Winter DR, Giladi A, Lara-Astiaso D, Levy M, Salame TM, Weiner A, David E, et al. (2016). The Spectrum and Regulatory Landscape of Intestinal Innate Lymphoid Cells Are Shaped by the Microbiome. Cell 166, 1231–1246 e1213. [PubMed: 27545347]

Hoveyda H, Brantis CE, Dutheuil G, Zoute L, Schils D & Fraser G (2011). Compounds, pharmaceutical composition and methods for use in treating gastrointestinal disorders. . International Patent Application WO 2011/076732 A1.

Huang DW, Sherman BT, Tan Q, Collins JR, Alvord WG, Roayaei J, Stephens R, Baseler MW, Lane HC, and Lempicki RA (2007). The DAVID Gene Functional Classification Tool: a novel biological module-centric algorithm to functionally analyze large gene lists. Genome Biol 8, R183. [PubMed: 17784955]

Ibiza S, Garcia-Cassani B, Ribeiro H, Carvalho T, Almeida L, Marques R, Misic AM, Bartow-McKenney C, Larson DM, Pavan WJ, et al. (2016). Glial-cell-derived neuroregulators control type 3 innate lymphoid cells and gut defence. Nature 535, 440–443. [PubMed: 27409807]

Kim SH, Cho BH, Kiyono H, and Jang YS (2017). Microbiota-derived butyrate suppresses group 3 innate lymphoid cells in terminal ileal Peyer's patches. Sci Rep 7, 3980. [PubMed: 28638068]

Kinnebrew MA, Buffie CG, Diehl GE, Zenewicz LA, Leiner I, Hohl TM, Flavell RA, Littman DR, and Pamer EG (2012). Interleukin 23 production by intestinal CD103(+)CD11b(+) dendritic cells in response to bacterial flagellin enhances mucosal innate immune defense. Immunity 36, 276–287. [PubMed: 22306017]

Kiss EA, Vonarbourg C, Kopfmann S, Hobeika E, Finke D, Esser C, and Diefenbach A (2011). Natural aryl hydrocarbon receptor ligands control organogenesis of intestinal lymphoid follicles. Science 334, 1561–1565. [PubMed: 22033518]

Klose CS, and Artis D (2016). Innate lymphoid cells as regulators of immunity, inflammation and tissue homeostasis. Nat Immunol 17, 765–774. [PubMed: 27328006]

Klose CS, Kiss EA, Schwierzeck V, Ebert K, Hoyler T, d'Hargues Y, Goppert N, Croxford AL, Waisman A, Tanriver Y, and Diefenbach A (2013). A T-bet gradient controls the fate and function of CCR6-RORgammat+ innate lymphoid cells. Nature 494, 261–265. [PubMed: 23334414]

Koh A, De Vadder F, Kovatcheva-Datchary P, and Backhed F (2016). From Dietary Fiber to Host Physiology: Short-Chain Fatty Acids as Key Bacterial Metabolites. Cell 165, 1332–1345. [PubMed: 27259147]

Korn T, Bettelli E, Oukka M, and Kuchroo VK (2009). IL-17 and Th17 Cells. Annu Rev Immunol 27, 485–517. [PubMed: 19132915]

Le Poul E, Loison C, Struyf S, Springael JY, Lannoy V, Decobecq ME, Brezillon S, Dupriez V, Vassart G, Van Damme J, et al. (2003). Functional characterization of human receptors for short chain fatty acids and their role in polymorphonuclear cell activation. J Biol Chem 278, 25481–25489. [PubMed: 12711604]

Longman RS, Diehl GE, Victorio DA, Huh JR, Galan C, Miraldi ER, Swaminath A, Bonneau R, Scherl EJ, and Littman DR (2014). CX(3)CR1(+) mononuclear phagocytes support colitis-

associated innate lymphoid cell production of IL-22. J Exp Med 211, 1571–1583. [PubMed: 25024136]

Love MI, Huber W, and Anders S (2014). Moderated estimation of fold change and dispersion for RNA-seq data with DESeq2. Genome Biol 15, 550. [PubMed: 25516281]

Maslowski KM, Vieira AT, Ng A, Kranich J, Sierro F, Yu D, Schilter HC, Rolph MS, Mackay F, Artis D, et al. (2009). Regulation of inflammatory responses by gut microbiota and chemoattractant receptor GPR43. Nature 461, 1282–1286. [PubMed: 19865172]

Mielke LA, Jones SA, Raverdeau M, Higgs R, Stefanska A, Groom JR, Misiak A, Dungan LS, Sutton CE, Streubel G, et al. (2013). Retinoic acid expression associates with enhanced IL-22 production by gammadelta T cells and innate lymphoid cells and attenuation of intestinal inflammation. J Exp Med 210, 1117–1124. [PubMed: 23690441]

Mowat AM, and Agace WW (2014). Regional specialization within the intestinal immune system. Nat Rev Immunol 14, 667–685. [PubMed: 25234148]

Nadkarni MA, Martin FE, Jacques NA, and Hunter N (2002). Determination of bacterial load by real-time PCR using a broad-range (universal) probe and primers set. Microbiology 148, 257–266. [PubMed: 11782518]

Nilsson NE, Kotarsky K, Owman C, and Olde B (2003). Identification of a free fatty acid receptor, FFA2R, expressed on leukocytes and activated by short-chain fatty acids. Biochem Biophys Res Commun 303, 1047–1052. [PubMed: 12684041]

Perry RJ, Peng L, Barry NA, Cline GW, Zhang D, Cardone RL, Petersen KF, Kibbey RG, Goodman AL, and Shulman GI (2016). Acetate mediates a microbiome-brain-beta-cell axis to promote metabolic syndrome. Nature 534, 213–217. [PubMed: 27279214]

Qiu J, Heller JJ, Guo X, Chen ZM, Fish K, Fu YX, and Zhou L (2012). The aryl hydrocarbon receptor regulates gut immunity through modulation of innate lymphoid cells. Immunity 36, 92–104. [PubMed: 22177117]

Rankin LC, Groom JR, Chopin M, Herold MJ, Walker JA, Mielke LA, McKenzie AN, Carotta S, Nutt SL, and Belz GT (2013). The transcription factor T-bet is essential for the development of NKp46+ innate lymphocytes via the Notch pathway. Nat Immunol 14, 389–395. [PubMed: 23455676]

Robinette ML, Fuchs A, Cortez VS, Lee JS, Wang Y, Durum SK, Gilfillan S, Colonna M, and Immunological Genome C (2015). Transcriptional programs define molecular characteristics of innate lymphoid cell classes and subsets. Nat Immunol 16, 306–317. [PubMed: 25621825]

Rooks MG, and Garrett WS (2016). Gut microbiota, metabolites and host immunity. Nat Rev Immunol 16, 341–352. [PubMed: 27231050]

Rutz S, Eidenschenk C, and Ouyang W (2013). IL-22, not simply a Th17 cytokine. Immunol Rev 252, 116–132. [PubMed: 23405899]

Sanos SL, Vonarbourg C, Mortha A, and Diefenbach A (2011). Control of epithelial cell function by interleukin-22-producing RORgammat+ innate lymphoid cells. Immunology 132, 453–465. [PubMed: 21391996]

Satoh-Takayama N, Vosshenrich CA, Lesjean-Pottier S, Sawa S, Lochner M, Rattis F, Mention JJ, Thiam K, Cerf-Bensussan N, Mandelboim O, et al. (2008). Microbial flora drives interleukin 22 production in intestinal NKp46+ cells that provide innate mucosal immune defense. Immunity 29, 958–970. [PubMed: 19084435]

Sawa S, Cherrier M, Lochner M, Satoh-Takayama N, Fehling HJ, Langa F, Di Santo JP, and Eberl G (2010). Lineage relationship analysis of RORgammat+ innate lymphoid cells. Science 330, 665–669. [PubMed: 20929731]

Sawa S, Lochner M, Satoh-Takayama N, Dulauroy S, Berard M, Kleinschek M, Cua D, Di Santo JP, and Eberl G (2011). RORgammat+ innate lymphoid cells regulate intestinal homeostasis by integrating negative signals from the symbiotic microbiota. Nat Immunol 12, 320–326. [PubMed: 21336274]

Serafini N, Vosshenrich CA, and Di Santo JP (2015). Transcriptional regulation of innate lymphoid cell fate. Nat Rev Immunol 15, 415–428. [PubMed: 26065585]

Smith PM, Howitt MR, Panikov N, Michaud M, Gallini CA, Bohlooly YM, Glickman JN, and Garrett WS (2013). The microbial metabolites, short-chain fatty acids, regulate colonic Treg cell homeostasis. Science 341, 569–573. [PubMed: 23828891]

Sonnenberg GF, and Hepworth MR (2019). Functional interactions between innate lymphoid cells and adaptive immunity. Nat Rev Immunol.

Sonnenberg GF, Monticelli LA, Elloso MM, Fouser LA, and Artis D (2011). CD4(+) lymphoid tissue-inducer cells promote innate immunity in the gut. Immunity 34, 122–134. [PubMed: 21194981]

Spits H, and Cupedo T (2012). Innate lymphoid cells: emerging insights in development, lineage relationships, and function. Annu Rev Immunol 30, 647–675. [PubMed: 22224763]

Tan JK, McKenzie C, Marino E, Macia L, and Mackay CR (2017). Metabolite-Sensing G Protein-Coupled Receptors-Facilitators of Diet-Related Immune Regulation. Annu Rev Immunol 35, 371–402. [PubMed: 28446062]

Vivier E, Artis D, Colonna M, Diefenbach A, Di Santo JP, Eberl G, Koyasu S, Locksley RM, McKenzie ANJ, Mebius RE, et al. (2018). Innate Lymphoid Cells: 10 Years On. Cell 174, 1054–1066. [PubMed: 30142344]

Wang F, Flanagan J, Su N, Wang LC, Bui S, Nielson A, Wu X, Vo HT, Ma XJ, and Luo Y (2012). RNAscope: a novel in situ RNA analysis platform for formalin-fixed, paraffin-embedded tissues. J Mol Diagn 14, 22–29. [PubMed: 22166544]

Withers DR, and Hepworth MR (2017). Group 3 Innate Lymphoid Cells: Communications Hubs of the Intestinal Immune System. Front Immunol 8, 1298. [PubMed: 29085366]

Withers DR, Hepworth MR, Wang X, Mackley EC, Halford EE, Dutton EE, Marriott CL, Brucklacher-Waldert V, Veldhoen M, Kelsen J, et al. (2016). Transient inhibition of ROR-gammat therapeutically limits intestinal inflammation by reducing TH17 cells and preserving group 3 innate lymphoid cells. Nat Med 22, 319–323. [PubMed: 26878233]

Zheng Y, Valdez PA, Danilenko DM, Hu Y, Sa SM, Gong Q, Abbas AR, Modrusan Z, Ghilardi N, de Sauvage FJ, and Ouyang W (2008). Interleukin-22 mediates early host defense against attaching and effacing bacterial pathogens. Nat Med 14, 282–289. [PubMed: 18264109]

Highlights

- Ffar2 agonsim promotes colonic ILC3 expansion and function.
- Ffar2 regulates colonic ILC3 proliferation and IL-22 production.
- Ffar2-deficient ILC3s enhance susceptibility to colonic inflammation and infection.
- Ffar2 agonism regulates ILC3-derived IL-22 via AKT and STAT3 signaling.

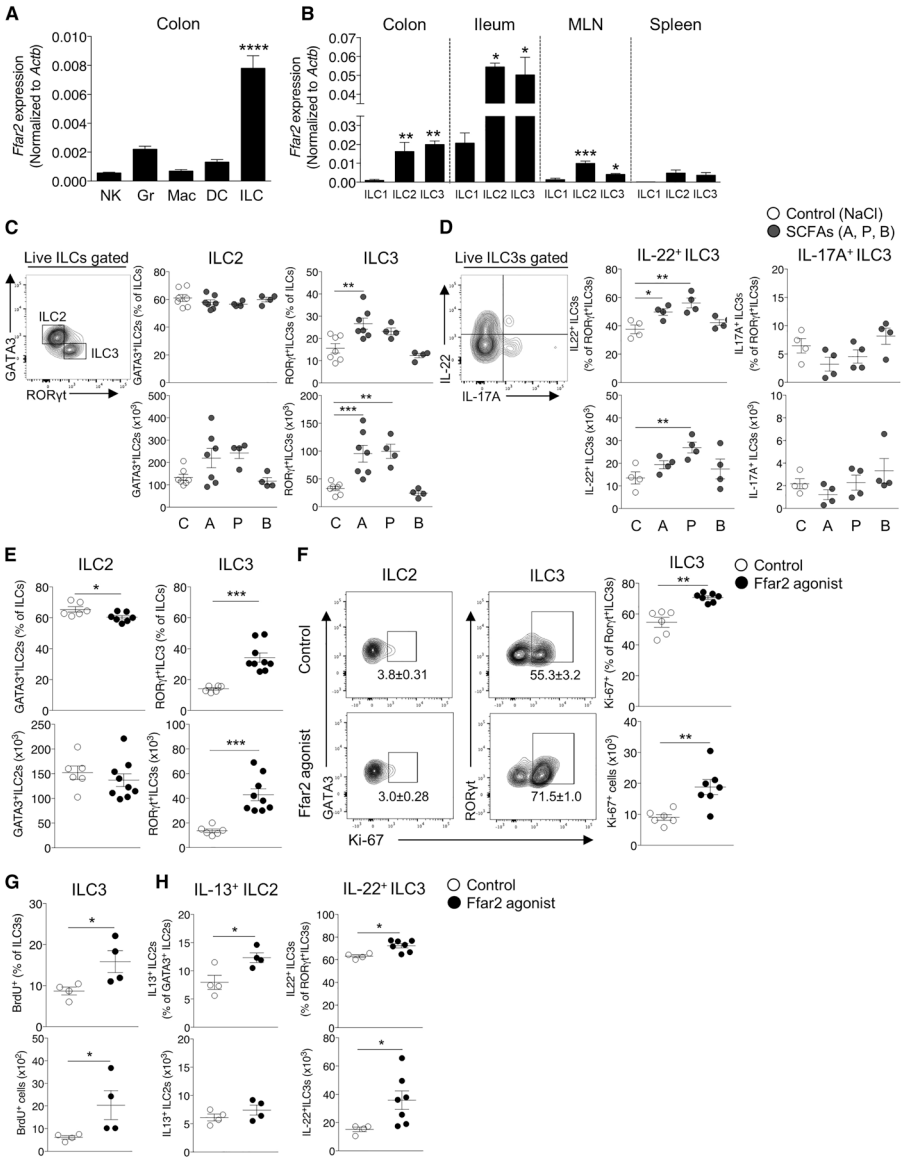

Figure 1. Ffar2 agonism selectively promotes colonic ILC3 expansion and function.

(A) *Ffar2* mRNA expression in mouse colonic cell populations (n=6 mice pooled per cell type per experiment). NK(conventional NK cells), G(granulocytes), Mac(macrophages), DC(conventional dendritic cells), and ILC(innate lymphoid cells). (B) *Ffar2* mRNA expression of ILC subsets in colon, small intestine (ileum), MLN and spleen (n=6 mice pooled per cell subset per experiment). (C) Colonic GATA3$^+$ ILC2s and RORγt$^+$ ILC3s from mice fed SCFAs. C, NaCl (n=7); A, acetate (n=7); P, propionate (n=4); B, butyrate (n=4). (D) IL-22 and IL-17A production in colonic ILC3s from mice fed SCFAs (n=4 mice for each SCFA). (E) Colonic ILC2s and ILC3s from mice fed Ffar2 agonist (n=9) or control (n=6). (F) Ki-67 expression in colonic ILC2s and ILC3s from mice fed Ffar2 agonist (n=7) or control (n=6). Numbers in flow plots represent % of Ki-67$^+$ cells in each gate. (G) BrdU$^+$ colonic ILC3s from WT fed with Ffar2 agonist (n=4) or control (n=4). (H) Analysis of IL-13$^+$ ILC2s (n=4 per group) and IL-22$^+$ ILC3s (n=4, control; n=7, Ffar2 agonist) from

mice fed Ffar2 agonist. Each symbol (C–H) represents data from an individual mouse. Data reflect independent experiments: 2 (G), 3 (A–D, F, H) and 4 (E). Data (bars or horizontal lines) shown as the mean ± s.e.m. *p<0.05, **p<0.01, ***p<0.001, ****p<0.0001 (one-way ANOVA with Tukey's (A) or Dunnett's (B) multiple comparisons test, two-tailed Mann-Whitney U test (C–H)). See Figure S1.

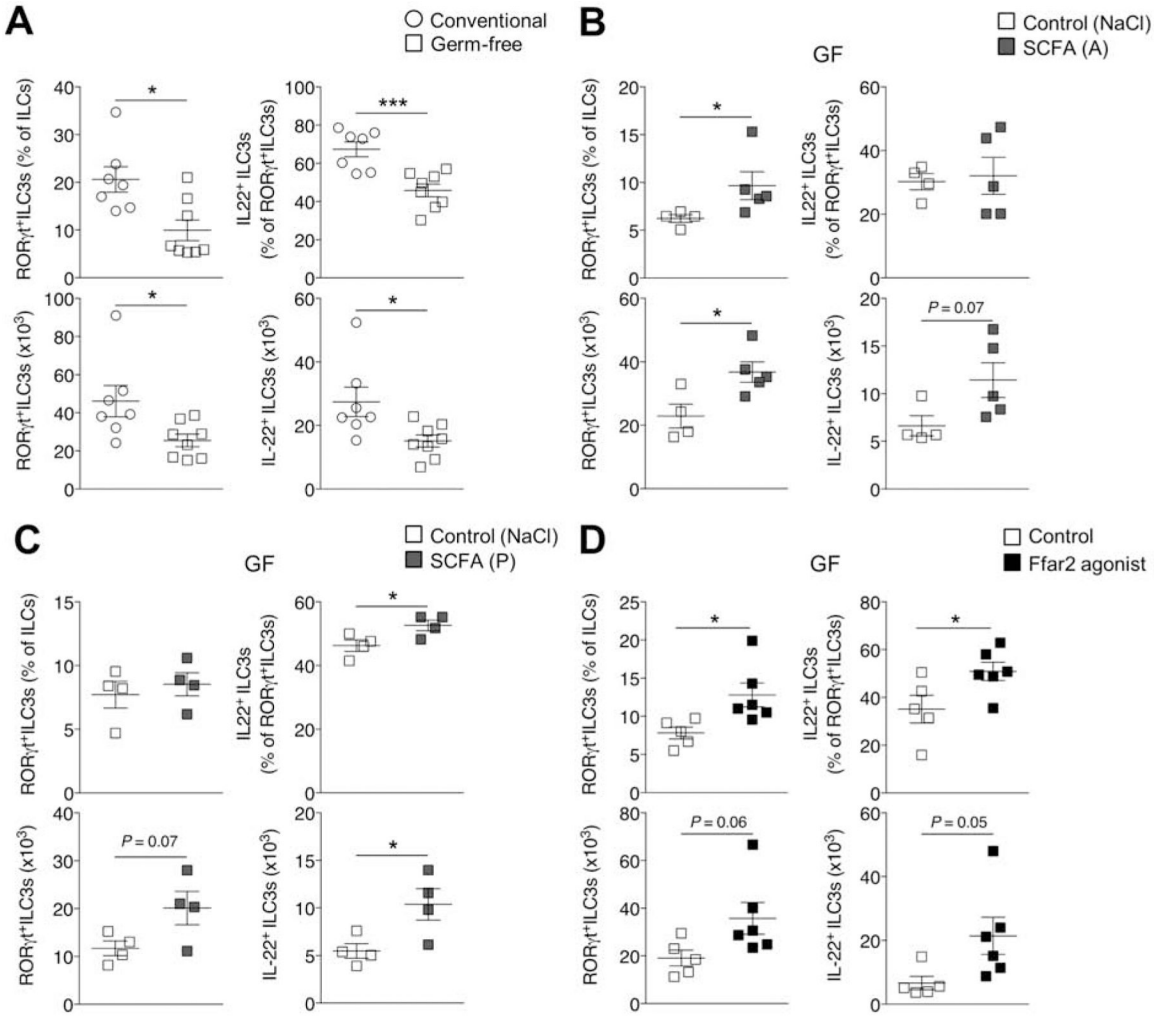

Figure 2. Microbiota influence colonic ILC3s and ILC3-derived IL-22 through Ffar2 agonism.

(A) Colonic ILC3s and IL-22$^+$ ILC3s from conventionally-reared SPF (n=7) or germ-free (GF) mice (n=8). (B) Colonic ILC3s and IL-22$^+$ ILC3s from GF mice fed acetate (n=5) or control (NaCl) (n=4) for 2 wks. (C) Colonic ILC3s and IL-22$^+$ ILC3s from GF mice fed propionate for 2 wks. Control (n=4); propionate (n=4). (D) Colonic ILC3s and IL-22$^+$ ILC3s from GF mice fed with Ffar2 agonist (n=6) or control (n=5) for 2 wks. Each symbol represents data from an individual mouse. Data reflect independent experiments: 3 (A), 2 in (B–D). Data show means ± s.e.m. *p<0.05, ***p<0.001, two-tailed Mann-Whitney U test.

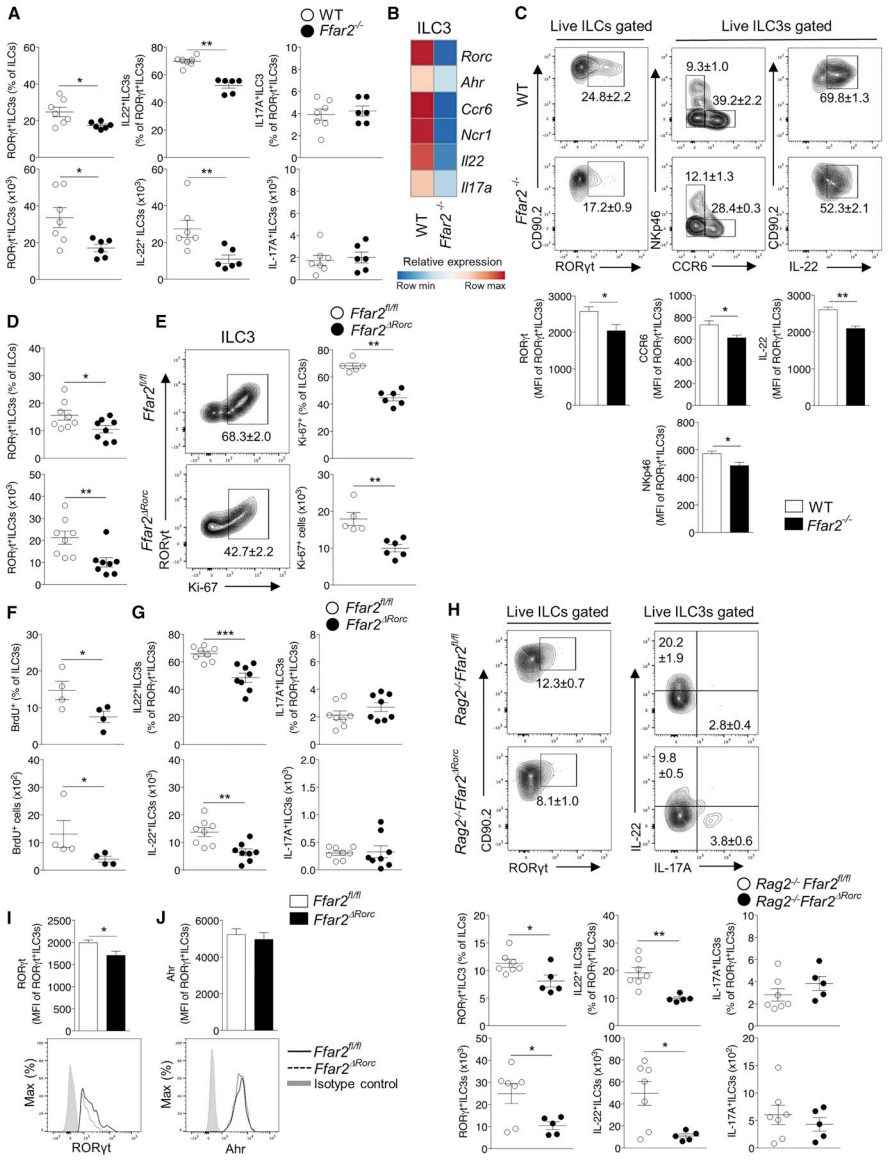

Figure 3. Ffar2 regulates colonic ILC3 proliferation and ILC3-derived IL-22 production.

(A) Colonic ILC3s, IL-22$^+$ ILC3s and IL-17A$^+$ ILC3s from *Ffar2*$^{-/-}$ (n=7) or littermate control (LC) WT mice (n=6). (B) Heatmap represents relative expression of select ILC3 signature genes. (C) Expressions of RORγt, CCR6, NKp46 and IL-22 in colonic ILC3s from *Ffar2*$^{-/-}$ (n=7) or LC WT mice (n=6). Flow plots represent population frequencies and bar graphs mean fluorescence intensities (MFIs). (D) Colonic RORγt$^+$ ILC3s from *Rorc-cre Ffar2*$^{fl/fl}$ (*Ffar2*$^{\Delta Rorc}$)(n=8) or LC *Ffar2*$^{fl/fl}$ mice (n=8). (E) Ki-67 expression in colonic ILC3s from *Ffar2*$^{\Delta Rorc}$ (n=6) or LC *Ffar2*$^{fl/fl}$ mice (n=5). (F) BrdU$^+$ colonic ILC3s from *Ffar2*$^{\Delta Rorc}$ (n=4) or LC *Ffar2*$^{fl/fl}$ mice (n=4). (G) IL-22 and IL-17A production in colonic ILC3s from *Ffar2*$^{\Delta Rorc}$ (n=8) or LC *Ffar2*$^{fl/fl}$ mice (n=8). (H) Colonic ILC3s, IL-22$^+$ ILC3s, IL-17A$^+$ ILC3s from *Rag2*$^{-/-}$*Ffar2*$^{\Delta Rorc}$ (n=5) compared to *Rag2*$^{-/-}$*Ffar2*$^{fl/fl}$ mice (n=7). Flow plots represent population frequencies. (I) RORγt expression in colonic ILC3s from *Ffar2*$^{\Delta Rorc}$ (n=9) or LC *Ffar2*$^{fl/fl}$ mice (n=8). Gray shaded area indicates isotype-matched

control antibody staining. Bar graph depicts RORγt MFI. (J) Intracellular Ahr expression in colonic ILC3s from *Ffar2*$^{\Delta Rorc}$ (n=9) or control *Ffar2*$^{fl/fl}$ mice (n=8). Each symbol (A, D–H) represents data from an individual mouse. Data reflect independent experiments: 4 in (D, G), 3 in (A, C, E, H), 2 in (F), or pooled from 4 (I, J). For RNA-seq (B), Data are pooled from 12 independent FACS sessions with cells harvested from 5–6 mice for *Ffar2*$^{-/-}$ (n=20) and control WT mice (n=30). Data (bars or horizontal lines) show mean ± s.e.m. *p<0.05, **p<0.01, ***p<0.001 (unpaired two-tailed Student's *t*-test (A, C, D, G–I), two-tailed Mann-Whitney U test (E, F) as these data were not normally distributed, this non-parametric test was employed). See Figures S2.

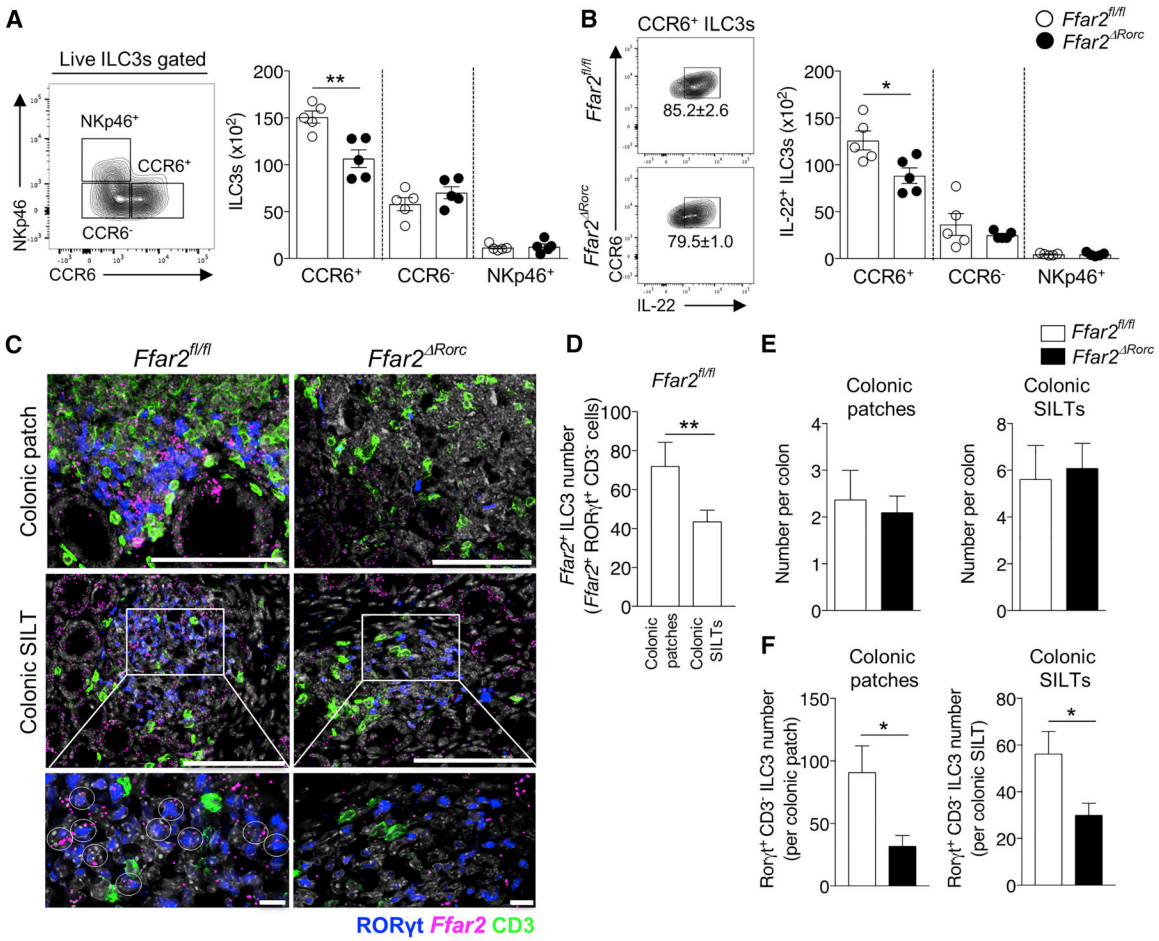

Figure 4. Ffar2 influences CCR6$^+$ ILC3 expansion and function.

(A) Colonic ILC3 subsets (CCR6$^+$, CCR6$^-$ and NKp46$^+$) in *Ffar2*$^{\Delta Rorc}$ (n=5) or littermate control (LC) *Ffar2*$^{fl/fl}$ mice (n=5). (B) IL-22$^+$ CCR6$^+$ ILC3s in *Ffar2*$^{\Delta Rorc}$ (n=5) or LC *Ffar2*$^{fl/fl}$ mice (n=5). (C–F) Distribution of Ffar2-expressing ILC3s in colonic lymphoid tissues of *Ffar2*$^{\Delta Rorc}$ (n=8) or LC *Ffar2*$^{fl/fl}$ mice (n=6). RNA *in situ* hybridization for Ffar2 transcripts (magenta) with immunofluorescence staining of CD3 (green) and RORγt$^+$ (blue) to identify ILC3s in colonic tissue sections (nuclei: gray). (C) Representative images of colonic ILC3s (RORγt$^+$ CD3$^-$ *Ffar2*$^+$ or RORγt$^+$ CD3$^-$ *Ffar2*$^-$) in a colonic patch (CP) and a colonic solitary intestinal lymphoid tissue (SILT) from *Ffar2*$^{\Delta Rorc}$ or *Ffar2*$^{fl/fl}$ mice (top, CPs; middle, colonic SILTs; bottom, high magnification images of colonic SILTs). Open circles represent Ffar2-expressing ILC3s (*Ffar2*$^+$ RORγt$^+$ CD3$^-$) in *Ffar2*$^{fl/fl}$ mouse colonic SILTs. Scale bars, 100 μm (top and middle); Scale bars, 10 μm (bottom). (D) Quantification of Ffar2-expressing ILC3s (*Ffar2*$^+$ RORγt$^+$ CD3$^-$) in colonic lymphoid tissues of *Ffar2*$^{fl/fl}$ mice. (E) Number of CPs and SILTs from *Ffar2*$^{\Delta Rorc}$ or littermate control *Ffar2*$^{fl/fl}$ mice. (F) Quantification of colonic ILC3s (RORγt$^+$ CD3$^-$) in lymphoid tissues of *Ffar2*$^{\Delta Rorc}$ or *Ffar2*$^{fl/fl}$ mice. Each symbol (A, B) represents data from an individual mouse. Data reflect independent experiments: 3 in (A, B) or combined from 4 in (C–F,). Data (bars) represent mean ± s.e.m. *p<0.05, **p<0.01 (two-tailed Mann-Whitney U test (A, B), unpaired two-tailed Student's *t*-test (D, F)). See Figure S3.

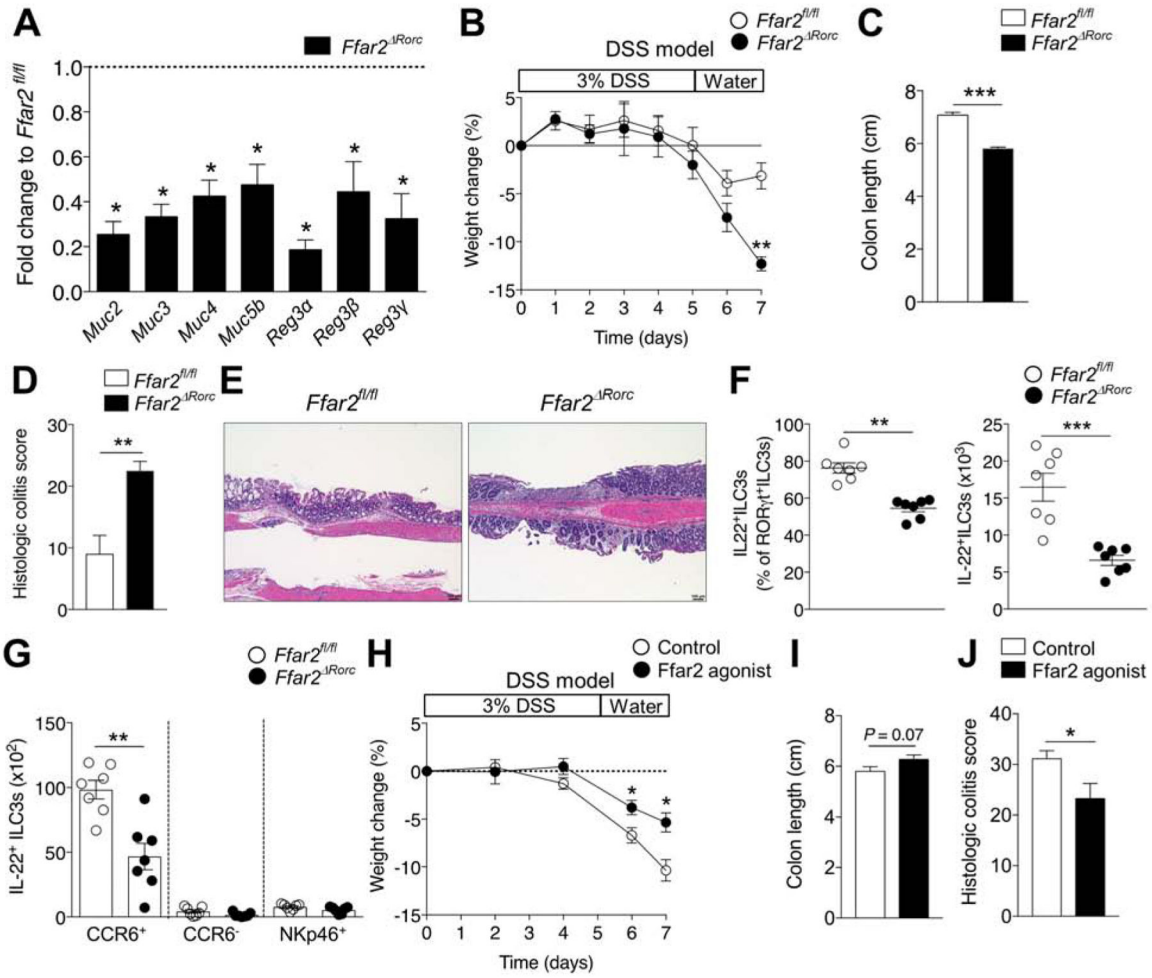

Figure 5. Ffar2 expression in ILC3s contributes to protection against DSS-induced colonic injury and inflammation.

(A) Gene expression in epithelial cells from *Ffar2*$^{\Delta Rorc}$ (n=7) compared to littermate control *Ffar2*$^{fl/fl}$ mice (n=6). (B–G) DSS model in *Ffar2*$^{\Delta Rorc}$ (n=12) and *Ffar2*$^{fl/fl}$ mice (n=12). (B) Body weight changes. (C) Colon length. (D) Histologic colitis score. (E) Representative light micrographs of colon sections. Scale bars, 100 μm. (F) Colonic IL-22^{+} ILC3s. (G) IL-22-producing ILC3 subsets. (H–I) DSS model in WT mice treated with Ffar2 agonist (n=5) or control (n=5). (H) Body weight changes. (I) Colon length. (J) Histologic colitis score. Each symbol (F, G) represents data from an individual mouse. Data reflect independent experiments: 2 (A, H–J), 3 (B–E), or 3 (F, G). Data (bars or horizontal lines) represent mean ± s.e.m. *p<0.05, **p<0.01, ***p<0.001(unpaired two-tailed Student's *t*-test (A–D, H–J), two-tailed Mann-Whitney U test (F, G)). See Figure S4.

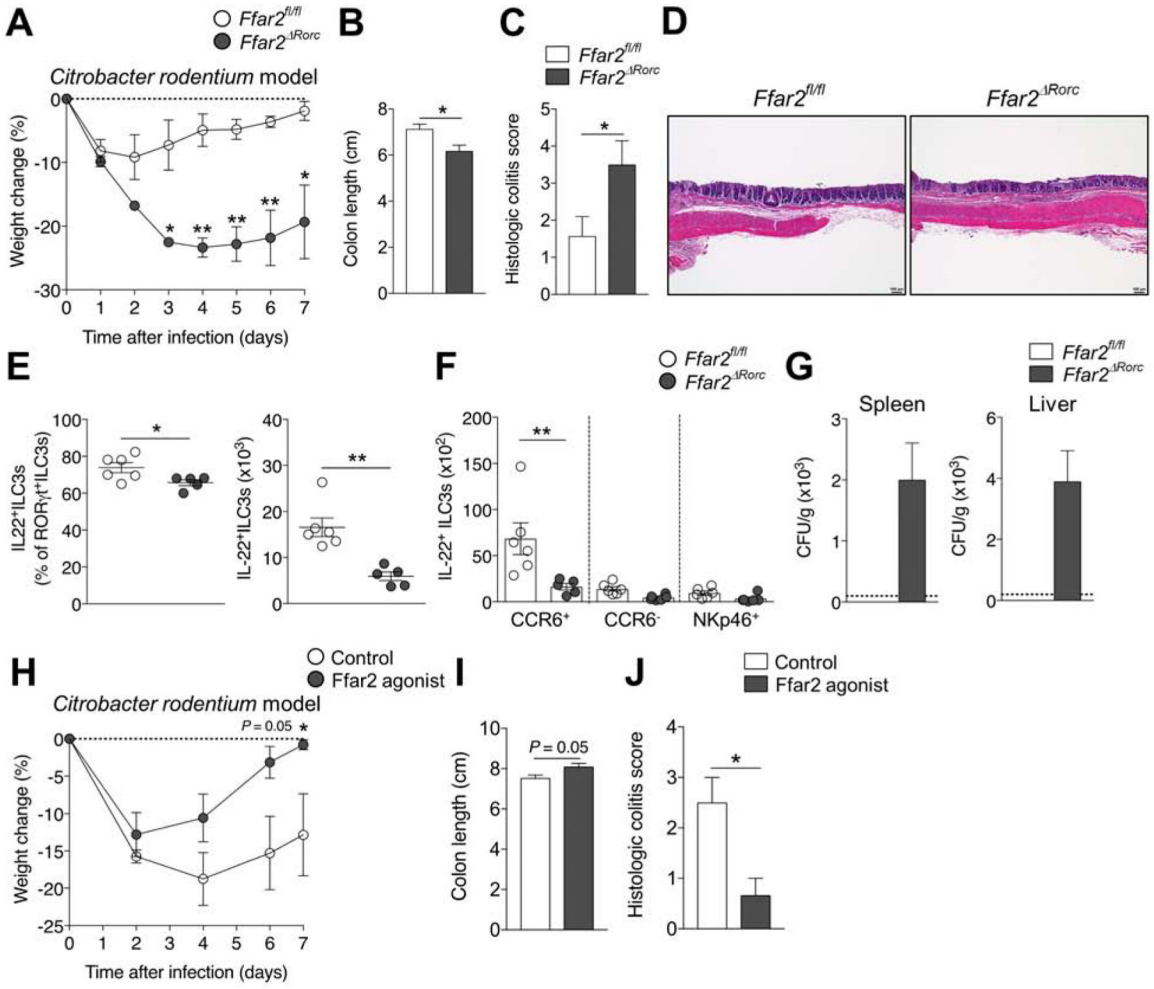

Figure 6. Ffar2 expression in ILC3s contributes to host defense against *C. rodentium* infection.

(A–G) *Ffar2*$^{\Delta Rorc}$ (n=15) and littermate control *Ffar2*$^{fl/fl}$ mice (n=14) were infected with *C. rodentium*. (A) Body weight changes. (B) Colon length. (C) Histologic colitis score. (D) Representative light micrographs of colon sections. Scale bars, 100 μm. (E) Colonic IL-22^{+} ILC3s. (F) IL-22-producing ILC3 subsets. (G) Bacterial load in spleen and liver on day 7. Dash lines indicate *C. rodentium* limit of detection. (H–J) WT mice pretreated with Ffar2 agonist (n=4) or control (N=4) prior to and during *C. rodentium* infection. (H) Body weight changes. (I) Colon length. (J) Histologic colitis score. Each symbol (E, F) represents data from an individual mouse. Data reflect independent experiments: 3 (A–D, G), 2 (H–J), or 3 (E, F). Data represent means ± s.e.m. *p<0.05, **p<0.01 (unpaired two-tailed Student's *t*-test (A–C, H–J), two-tailed Mann-Whitney U test (E, F)). See also Figure S5.

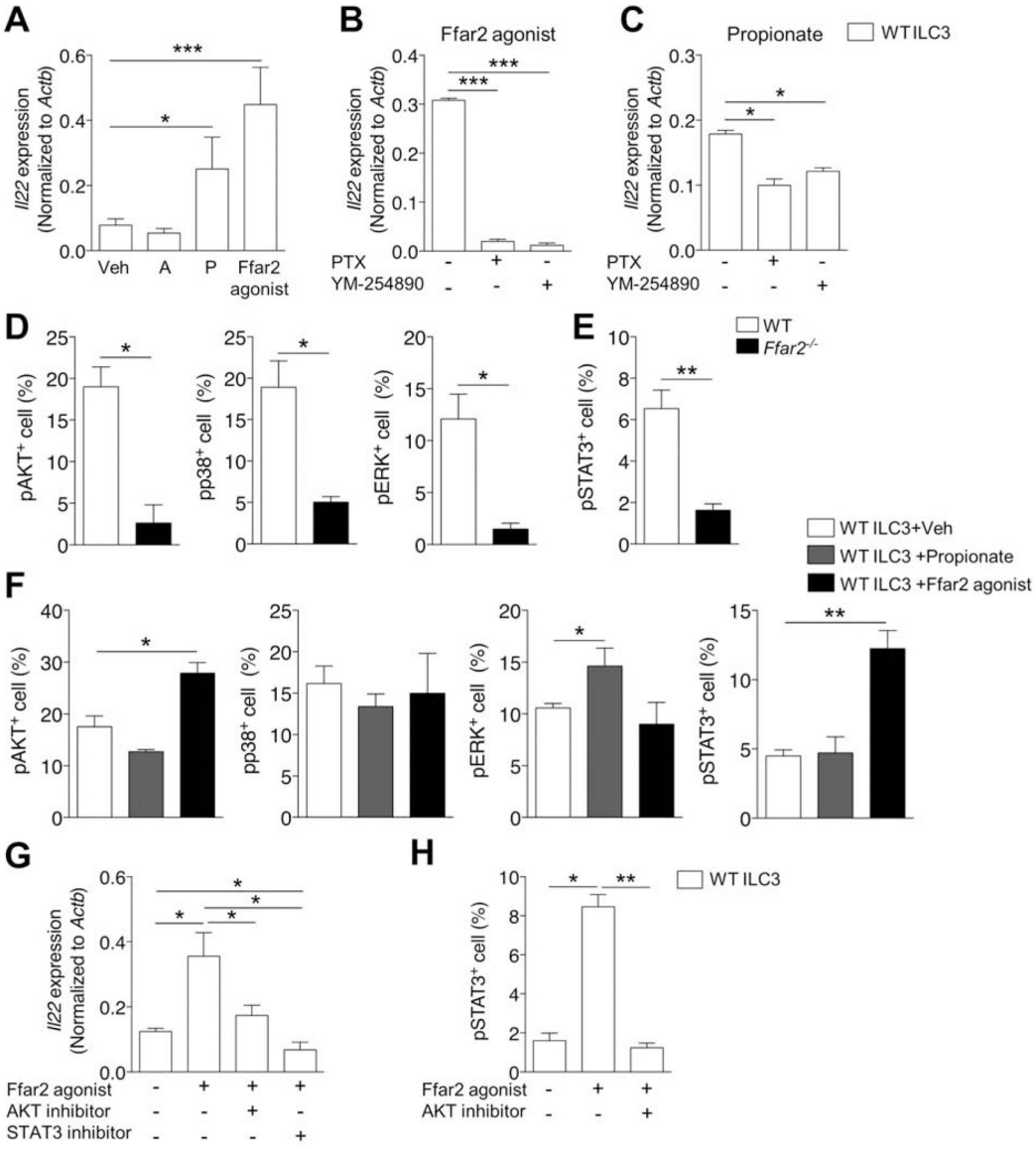

Figure 7. Ffar2 regulates colonic ILC3-derived IL-22 via AKT and STAT3 activation.

(A) *Il22* mRNA expression in sorted ILC3s cultured with acetate (A) (10 mM), propionate (P) (10 mM) or Ffar2 agonist (10 μM) (A, n=21; P, n=21; Ffar2 agonist, n=24). (B) *Il22* mRNA expression in sorted ILC3s cultured with Ffar2 agonist (10 μM), $G_{i/o}$ inhibitor (pertussis toxin, PTX) (500 ng/ml) or a G_q inhibitor (YM-254890) (1 μM) overnight. ($G_{i/o}$ inhibitor, n=24; G_q inhibitor, n=24) (C) *Il22* mRNA expression in sorted ILC3s cultured with P (10 mM), PTX (500 ng/ml) or YM-254890 (1 μM) overnight. (PTX, n=24; YM-254890, n=24) (D–G) Flow analysis of AKT, p38, ERK and STAT3 phosphorylation in sorted colonic ILC3s. (D) AKT, p38 and ERK phosphorylation in sorted colonic ILC3s from WT (n=20 for each protein) or *Ffar2*$^{-/-}$ mice (n=20 for each protein). (E) STAT3 activation in sorted colonic ILC3s from WT (n=24) or *Ffar2*$^{-/-}$ mice (n=24). (F) AKT, p38, ERK and STAT3 phosphorylation in sorted colonic ILC3s from mice cultured with P (10 mM) (n=21 for each protein) or Ffar2 agonist (10 μM) (n=24 for each protein). (G) *Il22* mRNA

expression in sorted ILC3s cultured with Ffar2 agonist (10 μM), AKT (10 μM) or STAT3 inhibitor (10 μM) (AKT inhibitor, n=24; STAT3 inhibitor, n=24). (H) STAT3 activation in sorted colonic ILC3s cultured with AKT inhibitor (10 μM) before stimulation with Ffar2 agonist (10 μM) (n=30). Data pooled from 4 independent experiments. Data reflect 3 independent flow cytometry sorting sessions with cells harvested from 5–7 mice per Ffar2 ligand (A), 4 independent FACS sessions with cells harvested from 6 mice per inhibitor (B, C, G), or 5–6 mice per protein (D, E, F, H). Data (bars) represent mean ± s.e.m. *$p<0.05$, **$p<0.01$ (two-tailed Student's *t*-test). See also Figure S6.

Key Resource Table

REAGENT or RESOURCE	SOURCE	IDENTIFIER
Antibodies		
Anti-mouse CD45 APC-Cy7 (30-F11)	BioLegend	Cat#:103116
Anti-mouse CD45 Pacific Blue (30-F11)	BioLegend	Cat#:103216
Anti-mouse CD90.2 (53–2.1) PE/Cy7	BioLegend	Cat#:140310
Anti-mouse CD90.2 (53–2.1) FITC	BioLegend	Cat#:140304
Anti-mouse Lineage markers Pacific Blue (17A2/RB6–8C5/ RA3–6B2/Ter-119/M1/70)	BioLegend	Cat#:133310
Anti-mouse CCR6 (29–21.17) PE	BioLegend	Cat#:129804
Anti-mouse CCR6 (29–21.17) APC	BioLegend	Cat#:129814
Anti-mouse NKp46 (29A1.4) FITC	BioLegend	Cat#:137606
Anti-mouse NKp46 (29A1.4) PerCP-eFluor710	eBioscience	Cat#:44-3351-82
Anti-mouse CD11b (M1/70) APC	BioLegend	Cat#:101212
Anti-mouse CD11c (N418) FITC	BioLegend	Cat#:117306
Anti-mouse CD103 (2E7) PE	eBioscience	Cat#:12-1031-81
Anti-mouse Gr-1 (RB6–8C5) PerCP/Cy5.5	BioLegend	Cat#:108426
Anti-mouse MHC class II (M5/114.15.2) PE	BioLegend	Cat#:107608
Anti-mouse MHC class II (M5/114.15.2) APC/Cy7	BioLegend	Cat#:107628
Anti-mouse NK1.1 (PK136) PE/Cy7	BioLegend	Cat#:108714
Anti-mouse NK1.1 (PK136) Pacific Blue	BioLegend	Cat#:108722
Anti-mouse KLRG1 (2F1) PE	BioLegend	Cat#:138408
Anti-mouse CD3ε (145–2C11) PE/Cy7	BioLegend	Cat#:100320
Anti-mouse CD4 (GK1.5) APC/Cy7	BioLegend	Cat#:100414
Anti-TCR gamma delta (GL-3) APC	eBioscience	Cat#:17-5711-82
Anti-mouse/rat RORgt (B2D) PE	eBioscience	Cat#:12-6981-82
Anti-mouse/rat RORgt (B2D) APC	eBioscience	Cat#:17-6981-82
Anti-mouse GATA3 (L50–823) Alexa Fluor 488	BD Biosciences	Cat#:560077
Anti-mouse Ahr (4MEJJ) APC	eBioscience	Cat#:50-5925-82
Anti-mouse T-bet (4B10) PerCP/Cy5.5	BioLegend	Cat#:644806
Anti-mouse Foxp3 (FJK-16s) PE	eBioscience	Cat#:12-5773-82
Anti-mouse Ki-67 (SolA15) PerCP-eFluor 710	eBioscience	Cat#:46-5698-80
Anti-mouse IL-22 (1H8PWSR) PerCP-eFluor 710	eBioscience	Cat#:46-7221-82
Anti-mouse IL-17A (eBio17B7) Alexa Fluor 488	eBioscience	Cat#:53-7177-81
Anti-mouse IL-13 (eBio13A) eFluor 660	eBioscience	Cat#:50-7133-80
Anti-mouse AKT(pS473) (D9E) APC	Cell Signaling Technology	Cat#:4075S
Anti-mouse p38 MAPK(pT180/pY182) (36/038) APC	BD Biosciences	Cat#:612595
Anti-mouse pERK1/2(pT202/pY204) (E10) APC	Cell Signaling Technology	Cat#:4375S
Anti-mouse STAT3(pY705) (4/p-STAT3) APC	BD Biosciences	Cat#:557815
Rabbit polyclonal anti-CD3 primary antibody	Abcam	Cat#:5690

REAGENT or RESOURCE	SOURCE	IDENTIFIER
Rat monoclonal anti- RORγt primary antibody	eBioscience	Cat#:14-6988-80
Goat anti- rat-HRP secondary antibody	Invitrogen	Cat#:A10549
Donkey anti-rabbit-HRP secondary antibody	Jackson ImmunoResearch	Cat#:711-035-152
Bacterial and Virus Strains		
Citrobacter rodentium	Laboratory of Dr. John Leong (Tufts University School of Medicine)	DBS100 strain
Chemicals, Peptides, and Recombinant Proteins		
Ffar2 agonist	EPICS SA, Belgium (Hoveyda, 2011)	Compound 1 in patent no. WO 2011/076732 A1
Sodium Acetate	Sigma-Aldrich	S8750
Sodium Propionate	Sigma-Aldrich	P5436
Sodium Butyrate	Sigma-Aldrich	303410
Dithiothreitol	Sigma-Aldrich	00-5523-00
Penicillin/streptomycin	Corning	30–002-CI
Collagenase D	Roche	11088882001
Collagenase A	Roche	10103586001
DNase I	Roche	10104159001
Dispase	StemCell Technologies	07913
Phorbol mysristate acetate (PMA)	Sigma-Aldrich	P8139–1MG
Ionomycin	Sigma-Aldrich	I0634–1MG
Brefeldin A Solution	BioLegend	420601
QIAzol	Qiagen	79306
RNAlater	Sigma-Aldrich	R0901–100ML
Mm-Ffar2 probe	ACDBio	433711
TSA cyanine 3	PerkinElmer	NEL744E001KT
TSA cyanine 5	PerkinElmer	NEL745E001KT
Prolong Gold antifade mounting medium	Life Technologies	P36934
FITC dextran	Sigma-Aldrich	46944–500MG-F
DSS	Thermo Scientific	J1448922
Pertussis Toxin	Calbiochem	CAS 70323-44-3
YM-254890	Focus Biomolecules	10-1590-0100
AKT1/2 kinase inhibitor (VIII)	Sigma-Aldrich	A6730–5MG
ERK kinase inhibitor (PD98059)	Sigma-Aldrich	P215–1MG
STAT3 inhibitor (S3I-201)	Sigma-Aldrich	SML0330–5MG
Critical Commercial Assays		
Live/Dead Fixable yellow dead cell stain kit	Invitrogen	L34959
Foxp3 Fix/Perm Buffer Set	BioLegend	421403
BD Phosflow Perm Buffer III	BD Bioscience	558050
BD Cytofix Fixation Buffer	BD Bioscience	554655
iScript Reverse Transcription Supermix	Bio-Rad	1708891

REAGENT or RESOURCE	SOURCE	IDENTIFIER
SYBR FAST Universal qPCR Master Mix	KAPA Biosystems	KK4619
SMART-seq v4 kit	Takara Bio Inc.	640170
NextSeq 500/550 High Output Kit v2.5 (150 Cycles)	Illumina	20024907
RNAscope Multiplex Fluorescent Detection Kit v2	ACDBio	323100
APC BrdU Flow Kit	BD biosciences	552598
RNeasy Mini Kit	Qiagen	74106
RNeasy Micro Kit	Qiagen	74004
Deposited Data		
RNA-Seq	This paper	GEO accession number: GSE137508
Experimental Models: Organisms/Strains		
Mouse: *Ffar2*$^{-/-}$	UTSW	N/A
Mouse: *Ffar2*$^{fl/fl}$	Laboratory of Dr. Brian Layden (University of Illinois)	N/A
Mouse: *Rorc-Cre*	(Eberl and Littman, 2004)	N/A
Mouse: *Rag2*$^{-/-}$	The Jackson Laboratory	JAX: 008449
Mouse: *Rorc-Cre x Ffar2*$^{fl/fl}$	This study	N/A
Mouse: *Rag2*$^{-/-}$ *x Rorc-Cre x Ffar2*$^{fl/fl}$	This study	N/A
Oligonucleotides		
See Table S1 for list of quantitative RT-PCR primers	This paper	N/A
Software and Algorithms		
BD FACSDiva v6.2	BD Biosciences	N/A
FlowJo v10.4.2	Tree Star	N/A
Prism v7.0b	GraphPad	N/A
STAR aligner version 2.7	(Dobin et al., 2013)	https://github.com/alexdobin/STAR
HTSeq version 0.11.1.	(Anders et al., 2015)	https://github.com/bowhan/HTSeq-count
DESeq2 version 1.24.0	(Love et al., 2014)	https://bioconductor.org/packages/release/bioc/html/DESeq2.html
DAVID	(Huang et al., 2007)	https://david.ncifcrf.gov/summary.jsp
NSI-Element Basic Research software	Nikon	N/A
ImageJ v1.0	ImageJ	https://imagej.nih.gov/ij/